Geoarchaeology and geochronology of the Upper Palaeolithic site of Temereşti Dealu Vinii, Banat, Romania: Site formation processes and human activity of an open-air locality

Geoarchäologie und Geochronologie der jungpaläolithischen Fundstelle Temereşti Dealu Vinii, Banat, Rumänien: Natürliche und menschliche Einflüsse auf die Genese einer Freilandfundstätte

Wei Chu[1]*, Stephan Pötter[2], Adrian Doboş[3], Thomas Albert[1], Nicole Klasen[4], Alexandru Ciornei[3], Janina J. Bösken[2] & Philipp Schulte[2]

[1] Institute of Prehistoric Archeology, University of Cologne, Weyertal 125, 50923 Cologne, Germany; email: wchu@uni-koeln.de
[2] Department of Geography, RWTH Aachen University, Wüllnerstraße 5b, 52062 Aachen, Germany
[3] Department of Paleolithic Archaeology, "Vasile Parvan" Institute of Archaeology of the Romanian Academy, 11 Henri Coanda Street, Sector 1, 010667 Bucharest, Romania
[4] Institute of Geography, University of Cologne, Albertus-Magnus-Platz, 50923 Cologne, Germany

Abstract - This paper reports on the excavation of a Late Pleistocene site at Temereşti *Dealu Vinii* in Western Romania, one of only four sizeable lithic assemblages with similarities to the tradition known from open-air localities in this region. The site consists of a flint scatter covering an area of at least 15 square meters and is comprised of blade, bladelet and flake cores, knapping debris and retouched tools including endscrapers and burins. An interesting feature of Temereşti *Dealu Vinii* is that it is on the same river system as the Upper Palaeolithic sites of Românești and Coşava that are about 10 km upstream. Similarities in the tools and blade technology imply that the sites may have been roughly contemporary. Here, we report on new artifacts, geochemistry, grain size, GIS analysis and geochronology that point to a Holocene reworking of the site. It also highlights the importance of rivers to humans as communication routes in the Upper Palaeolithic in the region.

Zusammenfassung - *Dieser Artikel berichtet von der Ausgrabung der jungpleistozänen Fundstelle Temereşti Dealu Vinii im Westen Rumäniens. Die Fundstelle ist eine von insgesamt nur vier umfangreichen Sammlungen prähistorischer Steinwerkzeuge aus Freilandfundstellen in der Region, die sich ähnliche Traditionen hinsichtlich der Steingeräteherstellung teilen. Die Lokalität Temereşti weist eine Fundstreuung von Silices auf, die über einen Bereich von mindestens 15 Quadratmetern reicht. Die Sammlung beinhaltet Klingen, Lamellen, Kerne, Schlagabfälle und retuschierte Werkzeuge wie Kratzer und Stichel. Bemerkenswert ist die Lage von Temereşti an demselben Flusssystem wie die 10 km flussaufwärts liegenden jungpaläolithischen Fundstellen Românești und Coşava. Gemeinsamkeiten in der Werkzeug- und Klingentechnologie zeigen, dass die Fundstellen zeitgleich besiedelt waren. Unsere Analyse der Artefakte, Geochemie, Korngrößen, sowie GIS-gestützte Auswertung der Geomorphologie und die Geochronologie legen nahe, dass die Sedimente der Fundstelle holozän überprägt wurden. Außerdem wird gezeigt, dass Flüsse wichtige Kommunikationswege während des Jungpaläolithikums in der Region darstellten.*

Keywords - Aurignacian, (Epi-)Gravettian, early Upper Palaeolithic, site formation processes, granulometry, optically stimulated luminescence
Aurignacien, (Epi-)Gravettien, Jungpaläolithikum, Entstehungsprozesse, Granulometrie, optisch-stimulierte Lumineszenz

Introduction

The Banat of Romania and Serbia is an important region for Palaeolithic studies because of the numerous Late Pleistocene findspots and fossils found throughout (Tasić & Draşovean 2011). Though the region has remained understudied in past decades, recent interest has been renewed by the recognition of the deep antiquity of modern humans and the direct evidence of Neandertal hybridization from the fossils at the Peştera cu Oase found in the region

*corresponding author

(Fig. 1; Trinkaus 2003; Trinkaus et al. 2003a, 2009, 2012; Fu et al. 2015). Subsequent archaeological work focusing on the early Upper Palaeolithic led to re-evaluations of the lithic assemblages and the production of radiometric dates that verified the contemporaneity of the fossils and their potential association (Teyssandier 2004; Doboş et al. 2009; Anghelinu et al. 2012; Anghelinu & Niţă 2014; Chu et al. 2014; Sitlivy et al. 2014).

The Bega River catchment, a tributary of the Tisa/Danube, is the richest part of the Banat record with numerous excavated sites reported in the literature (e.g. Coşava, Românești, Curtea and other unsecure finds in the towns of Făget and Leucuşeşti and Românești Apa Cave; Mogoşanu, 1978). These sites represent dense accumulations of Late Pleistocene archaeological materials in a part of the European map that has few large findspots and are usually poorly understood (Chu 2018).

Background

The Palaeolithic open-air site of Temereşti *Dealu Vinii* (hereafter Temereşti) is located in central Western Romania at the periphery of the Poiana Ruscă Mountains approximately 1.5 km north of the Bega River between the villages of Temereşti and Sinteşti on the top of Vinii Hill (45.8785 N, 22.2286 E; 220 m above sea level (a.s.l.); Figs. 1 & 5).

At Temereşti, Quaternary sediments have been known above Miocene deposits, though the archaeological site was not discovered until recently when nearby sand exploitation prompted exploratory test trenches as part of a rescue excavation (Micle et al. 2015). There, four test trenches and a larger 15 square meter trench were excavated at the top of the hill and the authors reported a stratigraphic succession of four distinct clayey yellow geological layers grading

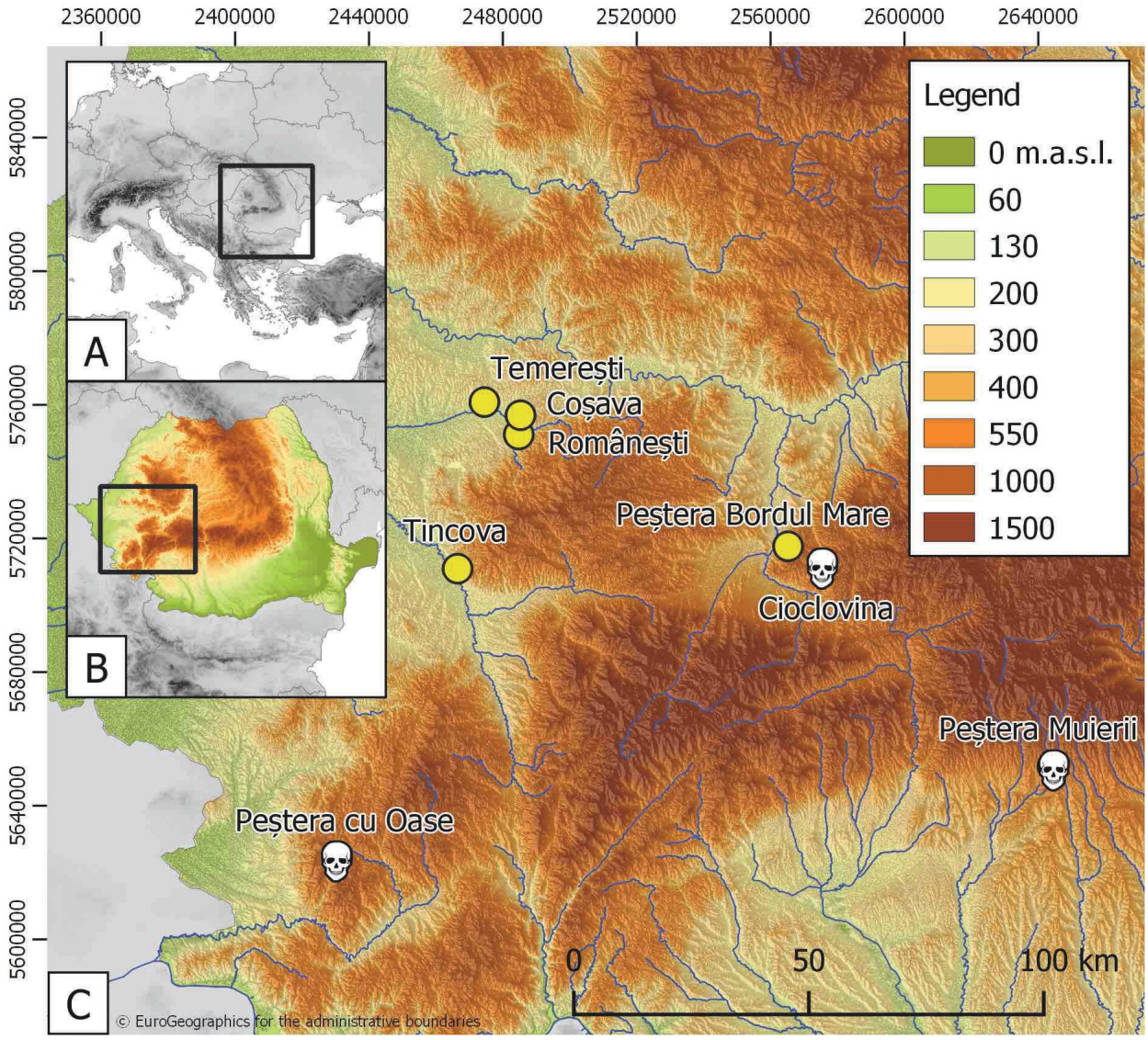

Fig. 1. Location of the site of Temereşti and other local early Upper Palaeolithic (yellow circles) and hominin sites (skulls) in the region. (A) is a European-wide projection, (B) is within Romania and (C) is a detailed regional map. Map projection is WGS 84 ESPG: 3857/Pseudo-Mercator.

Abb. 1. *Lage der Fundstelle Temereşti und weiterer jungpaläolithischer (gelbe Kreise) und Homininenfundstellen (Schädel) in der Umgebung. (A) Lage des Untersuchungsgebietes innerhalb Europas und (B) innerhalb Rumäniens. (C) zeigt das Untersuchungsgebiet im Detail.*

progressively to coarse sand (Layers I–IV from top to bottom; see Micle et al. 2015: 589, Figs. 1 & 2).

Lithic artifacts were reportedly found in their top three geological layers, to a maximum depth of 80 cm where in an expanded test trench, 278 lithics were recovered. Some artifacts were found in the layer immediately beneath the surface (N = 77), but most of lithics were recovered between about 40 and 55 cm (N = 169) suggesting that the site experienced limited taphonomic processes.

Cortical flakes were the most abundant artifacts though there were also fragmented blades and bladelets. Among the inventory were laminar cores, retouched flakes, blades and bladelets. Based on the typology and depth of the artifacts, the excavators indicated an archaeological succession corresponding to the geological layers with the first two representing late Upper Palaeolithic assemblages and last (Layer III) an early Upper Palaeolithic assemblage.

The site of Temereşti is of archaeological importance because:

1. Temereşti is a new point on the poorly understood map of Banat Aurignacian, that heretofore includes the sites of Românești, Coşava, Tincova and Crvenka-At near Vršac, Serbia (Fig. 1; e.g. Mogoşanu 1978; Chu et al. 2014).
2. Temereşti and the other Banat Aurignacian findspots are among the few sites geographically located between the early Aurignacian sites in the Swabian Jura and the Lower Danube and therefore are an integral part of falsifying the hypothesis that early modern humans in Europe used the Danube as a migration axis.
3. The results of the rescue excavation also provided a curious contrast to nearby Românești which produced few cortical pieces and a plethora of bladelets. Augmenting the collections from Temereşti would therefore permit understanding spatial and technological variation between two different sites in the same region.
4. Finally, the Banat sites represent the closest contemporary sites to the Peştera cu Oase, where some of Europe's oldest human fossils have been found without Palaeolithic artifacts. These sites therefore are the few that are able to contextualize the material cultures of these early pioneers in Europe.

Therefore, the goal of our excavation at Temereşti was to excavate the site with the following aims in mind.

1. Augment the lithic collection from Temereşti to evaluate the typo-technological succession of the site.
2. Obtain 3D measurements of the finds along with sedimentological analyses of the site to understand the depositional and post-depositional context of the artifacts and decode potential palimpsest formations.
3. Obtain radiometric dates for the site using radiocarbon and optically stimulated luminescence dating.
4. Compare the new assemblage to the recently re-excavated sites of Românești and Coşava to understand the technological variability in the Banat region between different well excavated sites.

Methods

In October 2017, a new trench was installed adjacent to the original rescue excavation trench with the aims to examine the stratigraphy, obtain new archaeological material and produce radiometric ages (Fig. 2). Four square meters were excavated at 2 cm spits to a depth of 50–70 cm (the top of the gravels). All objects above 5 mm were recorded with a total station and the collected sediments from quarter square meters were wet-sieved through 5 mm mesh for unrecovered artifacts. The subsequent lithic analyses focused on measuring artifacts (i.e. length, width, thickness and weight) and describing features specific to known archaeological cultures including technology and typology (*sensu* Demars 1992; Inizan et al. 1999).

Sedimentological sampling

Sediment samples were taken from the north-facing wall of the trench. The profile wall was cleaned with a trowel and sampling was conducted in 1 cm increments from top to bottom. The lowermost 16 cm and the uppermost 6 cm were sampled in lower resolution (2–4 cm) due to the brittleness of the material. Three samples for optically stimulated luminescence (OSL) dating and 18 samples for portable OSL (pOSL) measurements were taken at night using red light filtered headlamps and lightproof plastic bags and film containers. OSL samples were taken in 0.52 m, 0.42 m and 0.32 m depth; pOSL samples were collected at 4 cm increments.

Geochemical and sedimentological analyses

To determine the inorganic geochemical composition of the sediment samples, an energy dispersive X-ray fluorescence (EDPXRF) analysis using a Spetro Xepos device was performed. Samples were sieved to the silt fraction (<63 µm) and dried at 105 °C for 12 hours. For each sample, 8 g were homogenized with 2 g of Fluxana Cereox wax and pressed into pellets with a pressure of 19.2 MPa for 120 seconds. Each sample was measured twice and rotated 90° between the measurements to avoid matrix effects. Conspicuous samples, where both measurements differed significantly, were measured again in duplicate to avoid analytical anomalies. Element contents were calculated in oxide form.

For grain size analyses, samples were air-dried at 35 °C and sieved to the fine earth fraction (<2 mm) and two subsamples of each sample (0.1 and 0.3 g) were pre-treated with 0.7 ml H_2O_2 (30 %) at 70 °C for 12 hours.

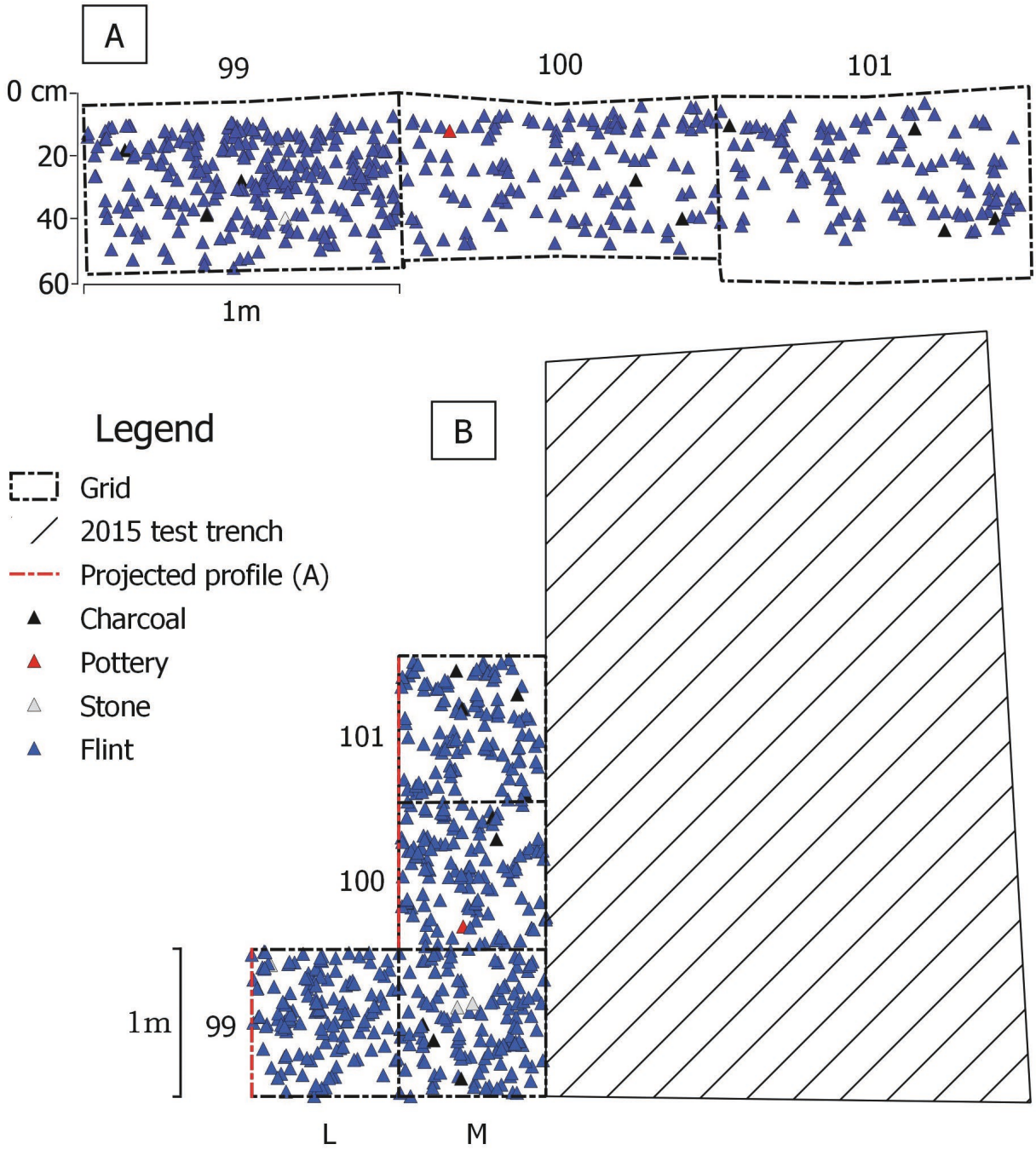

Fig. 2. Overview of find distributions from the 2017 excavation at Temereşti reported on in this paper. (A) Profile projection from the east and (B) Top-down projection including 2015 excavation outline (shaded, as seen after cleaning).

Abb. 2. *Überblick über die Fundverteilung der Ausgrabung in Temereşti 2017. (A) Profilprojektion von Osten und (B) Aufsicht der Grabung 2017 und Schnittgrenzen der Grabung 2015 (schraffiert, wie nach dem Putzen aufgefunden).*

This process was repeated until bleaching of the sample material was visible, but not longer than three days (Allen & Thornley 2004). To retain particle dispersement during the analysis, the samples were treated with 1.25 ml $Na_4P_2O_7 10H_2O$ (0.1 mol*l-^{1}) in an overhead shaker for 12 hours. The grain size was determined with a Beckman Coulter LS 13320 laser diffractometer using the Mie-theory (fluid RI: 1.33, sample RI: 1.55, imaginary RI: 0.1; Özer et al. 2010; Nottebaum et al. 2015; Schulte et al. 2016).

GIS analyses

The geomorphology of the site was investigated using the ALOS AW3D global digital surface model (DSM), provided by the Japan Aerospace Exploration Agency–Earth Observation Research Center (JAXA EORC, 2016). This elevation model (lateral resolution of c. 30 m) was used to generate contour lines (contour interval, 10 m; base height, 0 m) that were smoothed (smoothing tolerance 50 m; PAEK-algorithm). A polyline perpendicular to the contour lines was

vectorized, starting in the valley floor and following geomorphological features such as spurs and side valleys. The polyline was interpolated with the ALOS-DSM to obtain a cross section of the valley slope. A hill shade model (azimuth 315°, altitude 45°) was calculated for visualization and geomorphological discussion.

Geochronology

Laboratory treatment of the OSL samples included sieving to isolate the 100–150 µm fraction, HCl (10 %) to remove carbonates, H_2O_2 (10 %) to remove organic material and $Na_2C_2O_4$ (0.01 N) to remove clay and perform density separation (ρ = 2.62 g/cm^3 and ρ = 2.68 g/cm^3) to isolate quartz. We etched the quartz fraction with hydrofluoric acid (37 %, 40 minutes) and finally washed it with HCl (10 %, 1.0 hours). We used an automated Risø TL/OSL DA 20 reader equipped with a calibrated ^{90}Sr beta source. Blue-light emitting diodes (470 nm, FWHM = 20) and a Hoya U-340 filter (7.5 mm) transmitting wavelengths of 330 ± 40 nm were used for optical stimulation and signal detection of the multi-grain aliquots (1 mm diameter of the grain layer). The net OSL signal was obtained using the first 0.5 seconds of the stimulation and background subtraction of the last 4 seconds. We used the single-aliquot regenerative-dose approach (SAR) for all measurements (Murray & Wintle 2000, 2003) and measured the response to IR stimulation at the end of the SAR cycle (Duller 2003). For a preheat plateau test, we employed preheat temperatures between 180 and 280 °C for 10 seconds, a cutheat temperature of 20 °C below the preheat temperature and OSL stimulation for 40 seconds at 125 °C (1 mm, 4 aliquots each temperature, samples C-L3669 and C-L3671). Additionally, we carried out dose recovery tests of the same samples (given dose: 15 Gy (C-L4769), 9 Gy (C-L4770) and 6 Gy (C-L4771) after OSL stimulation for 100 seconds at room temperature) using preheat temperatures between 180 and 240 °C and a cutheat temperature that tracked the preheat temperature by –20 °C, respectively (1 mm, 5 aliquots). The mean dose was calculated using an arithmetic mean.

The radionuclide concentrations of the surrounding sediments were measured using high resolution gamma ray spectrometry. The dose rate was calculated using DRAC (Durcan et al. 2015) and included conversion factors of Guérin et al. (2011) and the measured water content. The cosmic dose rate was calculated following Prescott & Hutton (1994).

The 18 samples for luminescence profiling using a portable luminescence reader were measured twice. First, a batch of samples was measured without any sample preparation, using two replicates. All measurements were done using the same volume. Secondly, a samples batch was dried, crushed gently and two further replicates were measured to compare untreated and pretreated material. The measurements were done in a portable luminescence reader of the Scottish Universities Environmental Research Centre (SUERC) equipped with infrared (880 ± 40 nm) and blue (470 ± 20 nm) Light emitting-diode for signal stimulation, UG11 filters and a 25 mm bi-alkali photomultiplier for signal detection (cf. Sanderson & Murphy 2010). The measurement protocol comprised 60 seconds of infrared stimulation (IRSL), followed by 60 seconds of blue stimulation (BSL), separated by 15 seconds intervals to record the background (BG) (15 s BG, 60 s IRSL, 15 s BG, 60 s BSL, 15 s BG).

Additionally, Accelerator Mass Spectrometry (AMS) ^{14}C dating of a micro-charcoal (3.3 mg) sample found at a depth of 46 cm was carried out by Beta Analytic (Beta-484031) and calibrated using the INTCAL13 calibration curve (Bronk Ramsey et al. 2009; Reimer et al. 2013). The sample was pretreated by gentle crushing and dispersal in deionized water and then washed in hot acid (HCl), followed by alkali (NaOH) and acid solutions and finally dried.

Results

Geochemical and sedimentological analyses

Below the top humic layer (c. 5 cm), no clear stratigraphic units were identified until the appearance of a gravel layer c. 55 cm that graded into the covering sediments. Most of the geochemical proxies confirm the simple stratigraphy of the sampled profile. CaO, as a proxy for soluble compounds such as carbonates, shows a small increase just below the uppermost humic layer. In the silty material below, only slightly declining trends were visible, until the underlying fluvial sediments, where the values decrease rapidly. Many other (soluble) elements follow the same pattern, other chemical compounds show little to no variation at all (Fig. 3). The Al_2O_3/K_2O-ratio shows the clear distinction between the terrace sediment at the base of the profile and the silty material above. The ratio increases slightly with depth until 50 cm. Below, it increases rapidly demonstrating no large variation within the terrace sediment. The matrix of the fluvial package is characterized by redoximorphic features that were optically visible and are supported by the geochemical data.

On average, the grain sizes for the sequence are within the coarse silt fraction (median: 40 µm). The median grain size ranges from 31 µm in the silty material to 102 µm within the gravel-rich sediment. The grain size distributions throughout the section are tri-modal (Fig. 4). The first mode is in the range of medium to coarse silt. This particular mode is subdivided into two separated shoulders. Within the upper half of the profile, this peak is narrow, whereas the lower half of the profile shows a larger scatter. The second peak is in the fine to medium sand fraction. It is prominent and the scatter is narrow particularly in the upper half. In the lower half of the section, the percentages of this fraction are lower and singular samples show larger variation. The last and most

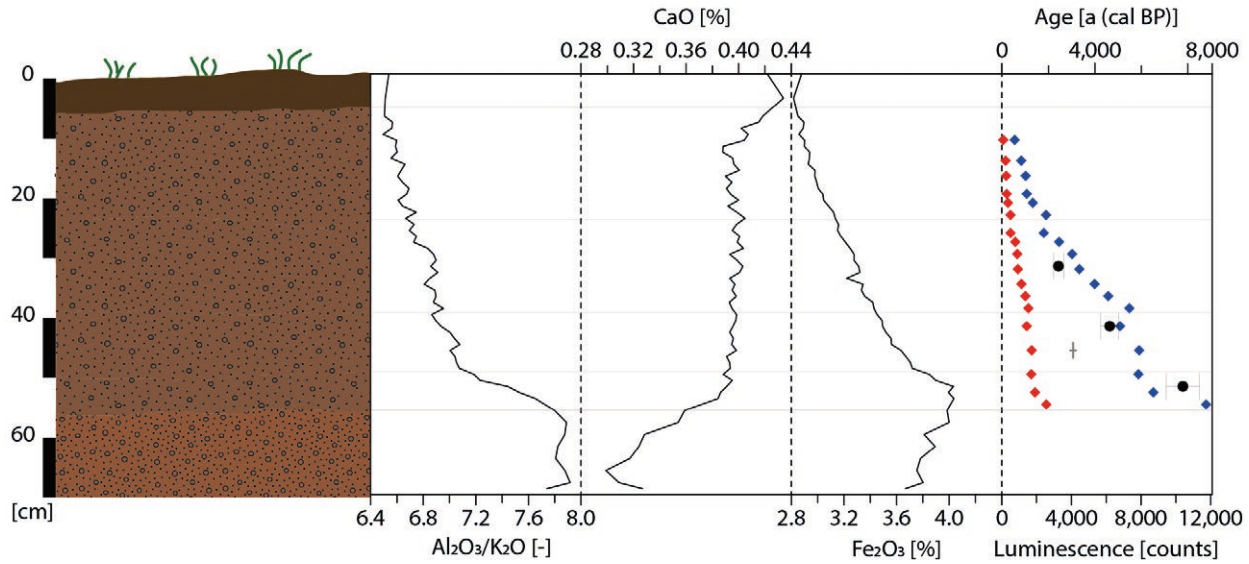

Fig. 3. Geochemical and dating results from Temereşti. Solid black lines: geochemical ratios (Al_2O_3/K_2O) and element contents (CaO, Fe_2O_3) as oxides. Red diamonds: luminescence intensities measured by pOSL for IRSL. Blue diamonds: luminescence intensities measured by pOSL for BSL. Gray cross: age range for radiocarbon dating of the charcoal sample found in 46 cm depth. Black circles: OSL ages (error bars indicate 1 σ uncertainty).

Abb. 3. *Ergebnisse der geochemischen und geochronologischen Untersuchungen für Temereşti. Durchgezogene schwarze Linien zeigen geochemische Verhältnisse (Al_2O_3/K_2O) und Elementgehalte (CaO, Fe_2O_3) in Oxidform. Rote Rauten zeigen die Lumineszenzintensität der pOSL für IRSL, blaue Rauten die Lumineszenzintensität der pOSL für BSL. Das graue Kreuz zeigt die Altersspanne der Radiokohlenstoffdatierung der in 46 cm Tiefe gefundenen Holzkohle. Die schwarzen Kreise zeigen die OSL-Alter mit Fehlerbalken (1 σ Unsicherheit).*

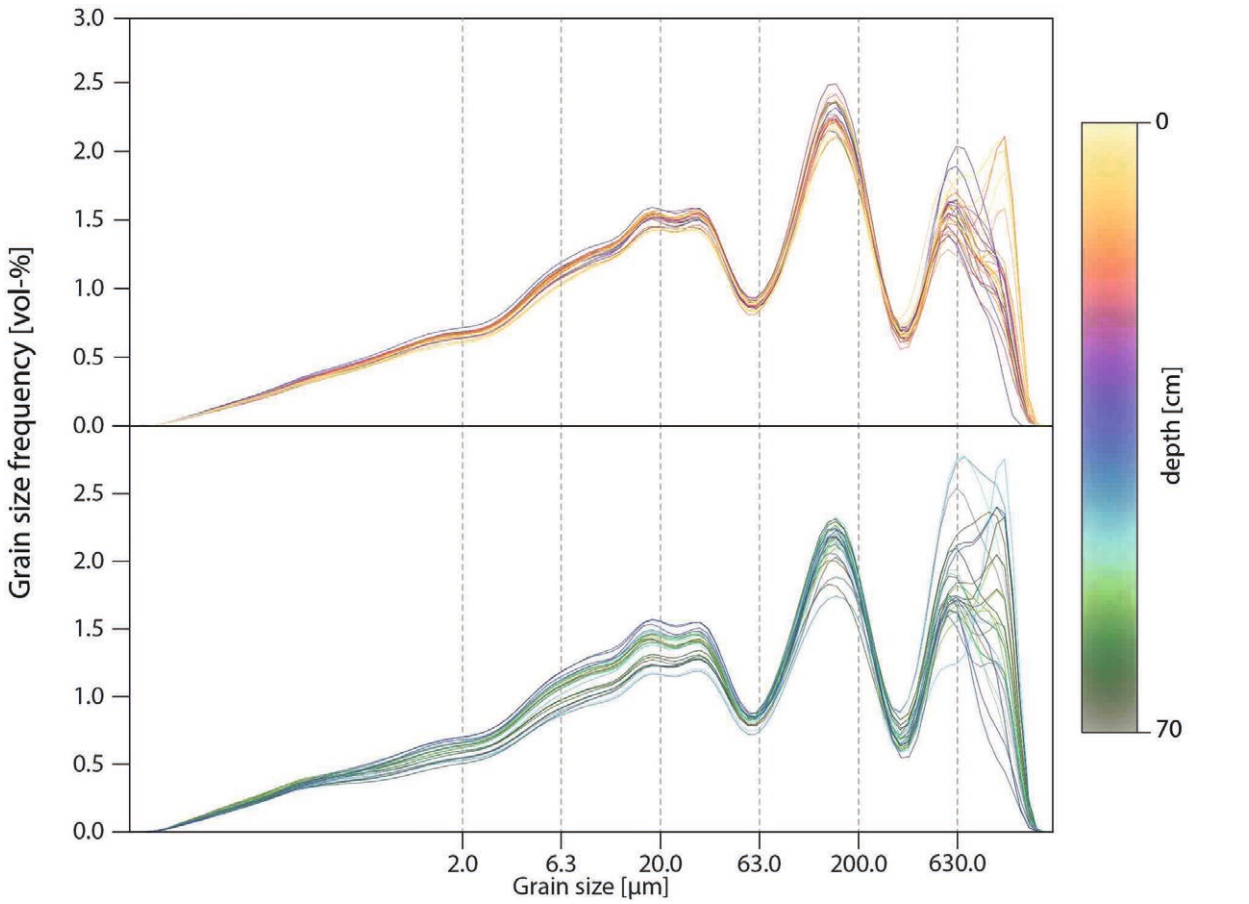

Fig. 4. Grain size distribution from Temereşti. The upper panel represents the upper half of the profile (0-35 cm); the lower panel the lower half (35-70 cm). Note the continuous depth scale color coding the depth of each sample.

Abb. 4. *Korngrößenverteilung für Temereşti. Das obere Feld zeigt die Ergebnisse aus der oberen Profilhälfte (0-35 cm), das untere Feld die der unteren Hälfte (35-70 cm). Die kontinuierliche Farbskala repräsentiert eine Farbkodierung der relativen Tiefe einer jeden Probe.*

complex mode is in the coarse sand fraction that is again subdivided in two major peaks. The mode is more prominent in the lower part. Also, the upper half is dominated by the finer of the two peaks, whereas the lower part is more complex and contains of more coarse particles.

GIS analyses

The geomorphology of the area is mainly influenced by fluvial processes of the Bega River and its tributaries (Fig. 5). The wide and flat alluvial plain of the Bega is bounded to the north by terrace edges. These edges are intersected by steep valleys of the tributaries of the Bega, mostly cut into the Pannonian sands underlying the Quaternary sediments. The cross section (Fig. 6) shows that the excavation site is situated on one of at least four terrace (like) levels of the valley. The terraces are flat and slightly tilted towards the river. They usually exceed several hundreds of meters in width. Some of the levels (especially levels T1, T2 and T5) are dissected by fluvial erosion.

Geochronology

The luminescence profiling revealed a constant increase of the blue and infrared signal downprofile (Fig. 3); there are almost no inversions visible. The increase is nearly linear and reaches a maximum of c. 12 000 counts for BSL and around 2 600 counts for IRSL. Standard errors between replicates are less than 15 %. The small grounding pretreatment increased the signals up to 35 % (increasing trend downprofile from 1 % in uppermost sample to 35 % in lowermost one). No changes are observed in the relative (normalized) signal. Data and signals are depicted in Supplementary Figs. 1-3).

The preheat plateau tests (Supplementary Fig. 4) that were carried out for all three OSL samples showed that the measured equivalent dose is independent of the temperature. For all samples, the laboratory dose was recovered with a measured/given dose ratio of 0.98 ± 0.02 (C-L4769), 1.05 ± 0.07 (C-L4770) and 1.07 ± 0.04 (C-L4771, Supplementary Fig. 4). According to the results of the preheat plateau tests and dose recovery tests, we used preheat temperatures of 240 °C (C-L4769), 260 °C (C-L4770) and 180 °C (C-L4771). The equivalent dose distributions (Supplementary Fig. 5) scatter with a relative standard deviation (RSD) of 67 % (C-L4769), 34 % (C-L4770) and 47 % (C-L4771). A representative dose response curve is depicted in Supplementary Fig. 6. An arithmetic mean equivalent dose of 15.2 ± 1.3

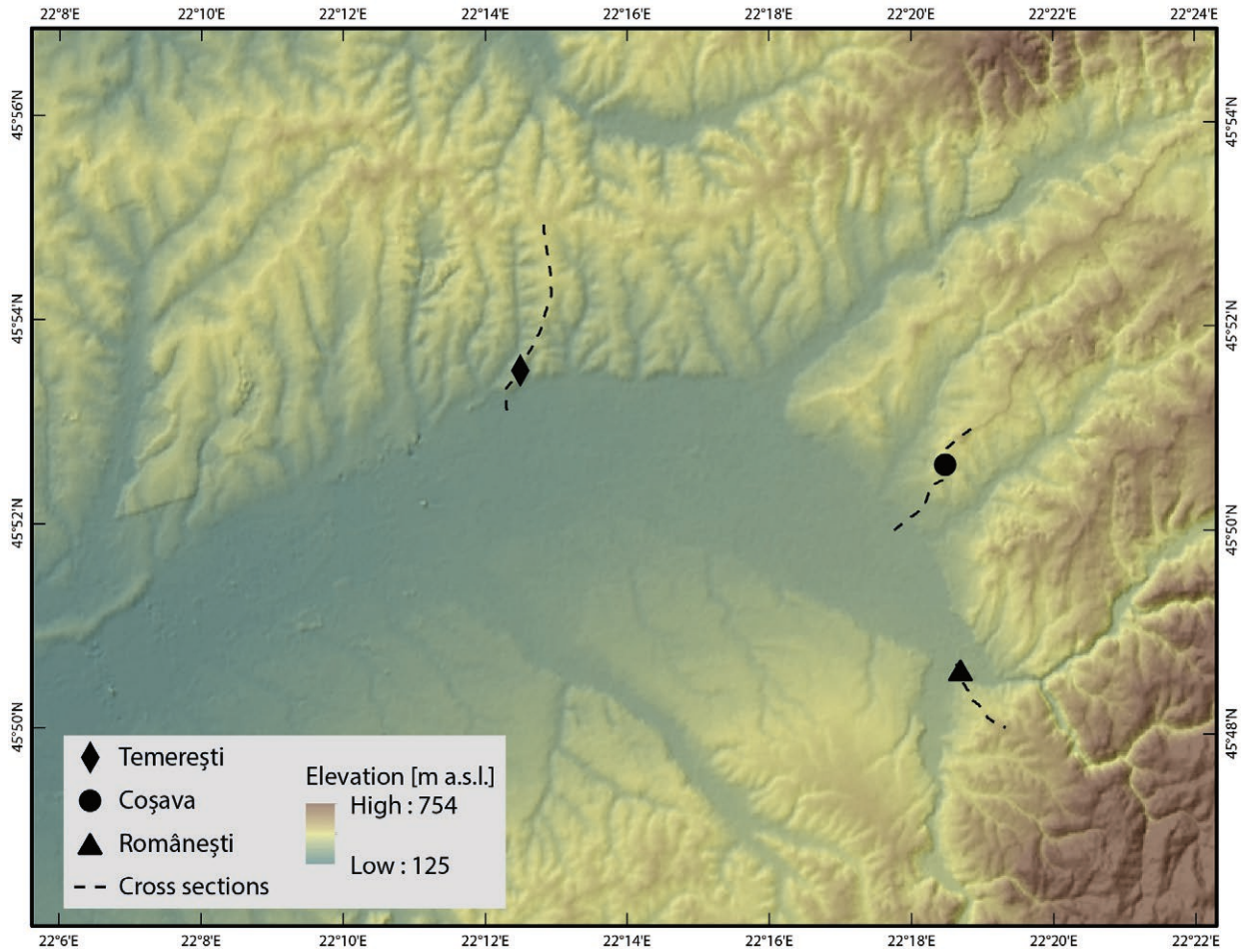

Fig. 5. Detailed topographic map of the Bega Valley. Dashed lines indicate the location of cross sections of figure 6.

Abb. 5. *Detaillierte topographische Karte des Begatals. Gestrichelte Linien zeigen die Lage der Querprofile in Abbildung 6.*

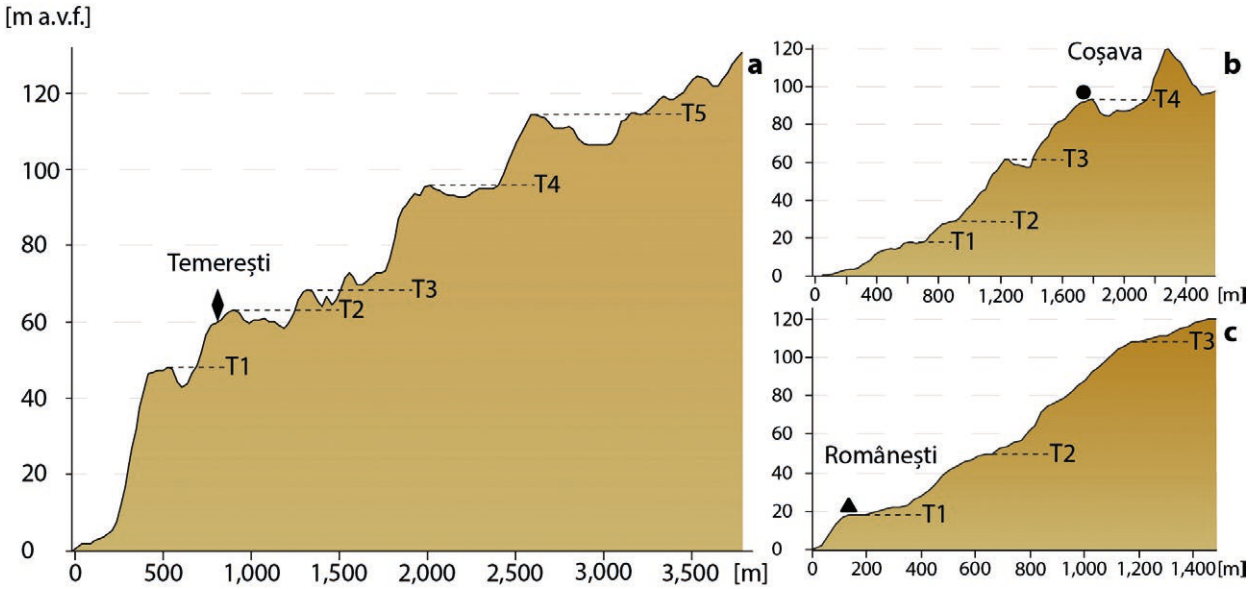

Fig. 6. Cross sections through the valley slopes at Temereşti, Coşava and Românești. Note that the terrace levels are numbered relatively for every site and not stratigraphically. Elevations are given in meter above valley floor [m a.v.f.].

Abb. 6. *Querprofile der Talhänge an den Fundstellen Temereşti, Coşava und Românești. Die Terrassenniveaus sind relativ für jedes Profil nummeriert und nicht stratigraphisch miteinander korreliert. Die Höhen sind in Metern über dem Talboden [m a.v.f.] angegeben.*

Gy (C-L4769), 9.42 ± 0.81 Gy (C-L4770) and 5.24 ± 0.46 Gy (C-L4771) was calculated and the resulting OSL ages are 7.79 ± 0.71 ka (C-L4769), 4.81 ± 0.42 ka (C-L4770) and 2.43 ± 0.22 ka (C-L4771; Fig. 7). Finally, the AMS ^{14}C dating of the charcoal sample (Beta-484031) found at a depth of 46 cm yielded a result of 3 158–2 960 calBP.

Utilized raw materials

The macroscopic determination of the raw materials for Temereşti assemblage (Fig. 8) was performed on a subset of 161 individually recorded pieces; generally, those larger than 1.5 cm in length (though some smaller pieces were also included) to ensure a large enough surface for diagnostic criteria to be identified (i.e. color, texture, inclusions, cortex type). Based on their macroscopic features, it was possible to differentiate several varieties of Banat flint (Comşa 1971), other siliceous rocks (OSR), quartzite (Qt) and vein quartz (VQt), siliceous mudstone/marlstone (MudSt) and a few varieties of "exotics". Artifacts with their entire surfaces covered by patina or macroscopic traits that did not allow for proper description and identification were grouped under an undetermined category of chert. Many pieces were partially or fully by whitish to mottled whitish-rosy-greyish or whitish-rosy (for some of the burned artifacts) patina. Various artifacts with macroscopic traits suggesting Banat flint, but which could not be assigned to one of the known varieties, were grouped in an undetermined category of Banat flint. During this analysis one conjoining was made.

Many artifacts exhibited traits of exposure to fire (in various degrees), covering a color range from reddish, rosy-reddish, whitish-reddish, rosy, brown and reddish, to greyish. Based on their macroscopic traits, all burned artifacts seem to be derived predominantly from Banat flint, while some derived from the other categories. The

Sample ID	Sample name	Sampling depth (m b.s.)	W (%)	n accepted/ measured aliquots	Radionuclide concentration U (ppm)	Th (ppm)	K (%)	Dose rate (Gy/ka)	De (Gy)	Age (ka)
C-L4769	TEME1	0.52	*3.8*	36/47	2.22 ± 0.10	7.99 ± 0.40	*0.92 ± 0.02*	1.95 ± 0.04	15.2 ± 1.34	7.79 ± 0.71
C-L4770	TEME2	0.42	*3.4*	42/47	2.22 ± 0.10	7.99 ± 0.40	*0.92 ± 0.02*	1.96 ± 0.04	9.42 ± 0.81	4.81 ± 0.42
C-L4771	TEME3	0.32	*3.6*	43/48	2.49 ± 0.12	8.42 ± 0.42	*1.01 ± 0.02*	2.16 ± 0.04	5.24 ± 0.46	2.43 ± 0.22

Fig. 7. Luminescence data showing the sample names, depth, measured water content (W), number of aliquots (n), radionuclide concentrations, dose rates, equivalent doses (De) and resulting ages.

Abb. 7. *Daten der Lumineszenzdatierungen mit Probennamen, Tiefen, gemessenem Wassergehalt, Anzahl der Aliquoten (n), Radionuklidkonzentrationen, Dosisleistung, Equivalenzdosen (De) und den daraus resultierenden Altern.*

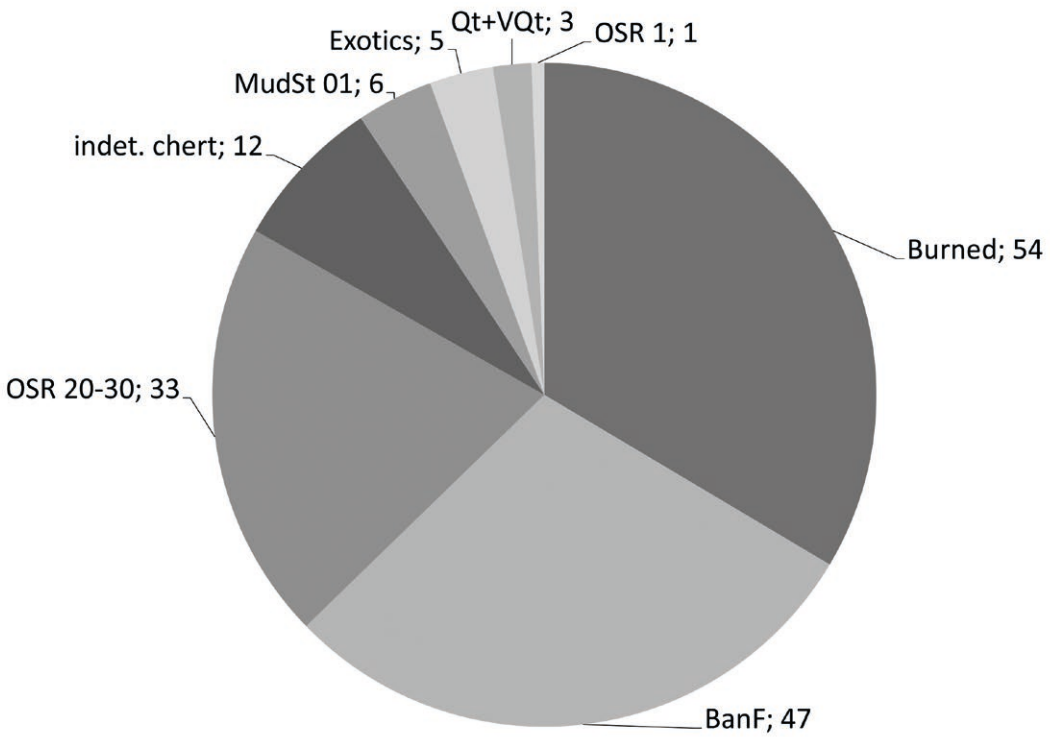

Fig. 8. Pie chart of sampled lithic raw material varieties and burned pieces.

Abb. 8. *Kreisdiagramm der beprobten lithischen Rohmaterialvarietäten und verbrannten Silices.*

influence of fire is indicated only by burned pieces (Fig. 8) as no combustion features were discovered. When examining the distribution across the four square meters, burned pieces were homogeneously distributed.

The analyzed artifacts exhibit different types of cortical surfaces:

1. "fresh" cortex represented by a yellowish-white carbonate rind (2–5 mm thick), slightly smoothened with a whitish, partially silicified, transitional area; observed only on some Banat flint pieces;
2. medium grained and porous beige-grey carbonate rind (5–10 mm thick), smoothened; identified on an artifact described as indeterminable chert;
3. neocortex (2–3 mm thick) indicating a very well smoothened carbonate rind, with a subcortical area suggesting transition from silica rich to unsilicified material; observed on pieces of Banat flint and OSR;
4. neocortex derived from very well smoothened surfaces, preserving or betraying the material's fabric; observed on pieces of Banat flint, burned, OSR and MudSt 01;
5. neocortex with transition from well smoothened areas to areas with abundant impact-point scars (generally associated with rounded or well-rounded pebbles/cobbles transported on long distances/or long time periods by water); observed on pieces of Banat flint, OSR, burned and Exo 53.

Cortex types 1, 3 and 4 can be associated on the same nodule/cobble as is the case of the ones collected from creeks in Poieni/Pietroasa area (Ciornei et al. in prep). Cortex types 3, 4 and 5 are indicative of alluvial gravels as evidenced by samples collected in gravels from the surrounding area (Temereşti, Coşava and Româneşti). Though siliceous rocks were found in the gravels directly under the geological deposit with artifacts, the pebbles are predominantly small sized (less than 5.5 cm in diameter).

Banat flint is widely available in secondary pre-Cenomanian continental deposits and Quaternary creek deposits in the area between Poieni and Pietroasa villages, but also in Miocene and Quaternary gravels starting from upstream Româneşti village up to Temereşti. Quartzite and vein quartz are omnipresent in all gravels of the area and well-represented in the metamorphic suite of the northwestern Poiana Ruscă Mountains. The MudSt 01 is macroscopically similar to a yellowish-brownish siliceous mudstone/marlstone identified in a gravel deposit on Carpenilor Valley near Breazova village (on the left side of Bega). OSR 1 was identified as a raw material characteristic to Căldărilor Valley (and its tributaries), east-southeast of Româneşti, but also found in the gravels of Bega Poieni.

With the mentioned exception, the broad category of OSR encompasses various siliceous rocks of unknown/undetermined genetic origin and not recognized in samples collected during the field surveys carried in the area around the Upper Palaeolithic sites from this area (Temereşti, Coşava and Româneşti).

Description of the lithic assemblage

The flint artifacts were found homogenously scattered throughout the profile from the surface of the excavation down to the basal gravels of the sequence with no clear patterning in terms of shape or size (Fig. 2). Larger artifacts (>2 cm) were systematically found in inclined positions between 30 and 90° to the ground surface.

A total of 1960 artifacts were recovered from the four square meter excavation of which 1 536 (78 %) were recovered from wet-sieving. The assemblage is dominated by flakes and debitage and to a lesser extent, blades and bladelets (Fig. 9).

Still, the cores are clearly oriented towards the production of blades and bladelets with larger flakes (>2 cm) comprising mostly technological pieces associated with core maintenance and crest production. Blade length averages 33.2 mm while bladelet length averages 17.4 mm with both maintaining a straight rectilinear profile (Fig. 10). Platforms for flakes were predominantly plain while those for bladelets and blades were predominantly linear or punctiform with intense platform abrasion and frequent lipping, suggesting soft hammer production for blades and bladelets (Fig. 11; *sensu* Debénath & Dibble 1994).

Out of the eight recovered cores, five were laminar; four of which were unidirectional (Fig. 12, M100-26; Fig. 13, M99-77) and one multidirectional). One (flake/residual) core was multidirectional (Fig. 12, M100-22), and the remaining two cores were undiagnostic. Seven out of eight cores have cortical surfaces below 40 %. The flake-to-core ratio (calculated according to Hiscock 2002) is 21.75, suggesting an intense core exploitation on site, testified as well by the presence of core rejuvenation flakes and large amount of debitage (Fig. 14, M100-43).

Debitage types	N single finds	N wet sieving	Total
Simple flakes	118	314	**432**
Core trimming flakes	7		**7**
Blades	85		**85**
Bladelets	67	175	**242**
Cores	8		**8**
Burin spalls	4		**4**
Shatter (chunk & debitage)	125		**125**
Indeterminate	10		**10**
Chips		1 047	**1 047**
Total	**424 (*21.6 %*)**	**1 536 (*78.4 %*)**	**1 960 (*100 %*)**

Fig. 9. Temereşti (2017) debitage assemblage divided between single finds and wet sieving finds.

Abb. 9. *Fundhäufigkeiten, unterteilt in Einzelfunde und Siebfunde für Temereşti (2017).*

Blank type		μ	σ
Complete flakes (62)	Length (mm)	27.9	16.9
	Width (mm)	19	11.5
	Thickness (mm)	7.8	6.0
	Weight (g)	7.7	15.5
Complete blades (8)	Length (mm)	33.2	14.4
	Width (mm)	15.8	8.6
	Thickness (mm)	5.0	3
	Weight (g)	3.5	4.6
Complete bladelets (20)	Length (mm)	17.4	4.5
	Width (mm)	7.6	2.3
	Thickness (mm)	3	1.4
	Weight (g)	0.4	0.4
Cores (8)	Length (mm)	51	21.4
	Width (mm)	33.4	14.7
	Thickness (mm)	21.7	10.1
	Weight (g)	53.3	61

Fig. 10. Mean (μ) and standard deviation (σ) of completely preserved flakes, blades and bladelets.

Abb. 10. *Mittelwerte (μ) und Standardabweichungen (σ) der vollständig erhaltenen Abschläge, Klingen und Lamellen.*

Retouched tools are few (N = 25), accounting for only 5.9 % of the lithic assemblage (Fig. 15). They are all manufactured on Banat flint and most (n = 18) are on non-cortical blanks. Among the 10 endscrapers, five are on flakes (including one on a core trimming flake and two on thick flakes; Fig. 14, M101-59) and four are on blades (Fig. 16, M99-71). A combination tool features an endscraper with a truncation (Fig. 16, M100-78). One blade endscraper (Fig. 16, M101-70) conjoined with the proximal part (Fig. 17, M101-71) of a retouched blade that was found next to it. Two burins on break (Fig. 14, M101-28) were also recovered.

In total, 12 retouched blades and bladelets were

Platform type	Blank type			
	Flakes	Blades	Bladelets	Total
Plain	37	5	1	**43**
Linear	9	20	11	**40**
Punctiform	8	9	18	**35**
Cortical	9	2	2	**13**
Crushed	2	1	1	**4**
Faceted	8	0	0	**8**
Dihedral	1	0	0	**1**
Indeterminate	12	8	9	**29**
Total	**86**	**45**	**42**	**173**

Fig. 11. Platform types of proximally preserved blank types (*sensu* Debénath & Dibble 1994: 14).

Abb. 11. *Schlagflächenarten proximal erhaltener Grundformen (sensu Debénath & Dibble 1994: 14).*

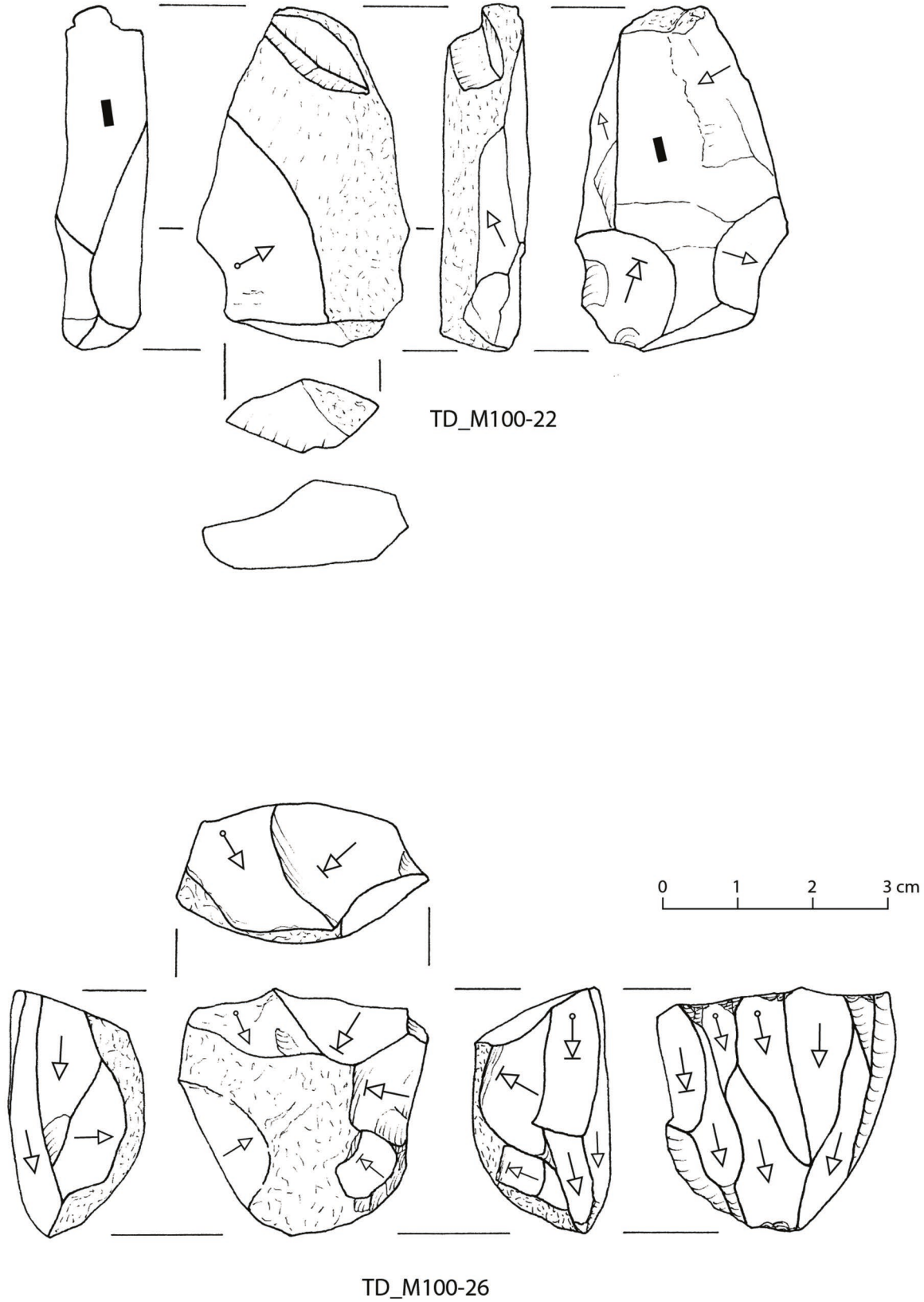

Fig. 12. Selection of cores from the 2017 excavation.
Abb. 12. *Auswahl von Kernen der Grabung 2017.*

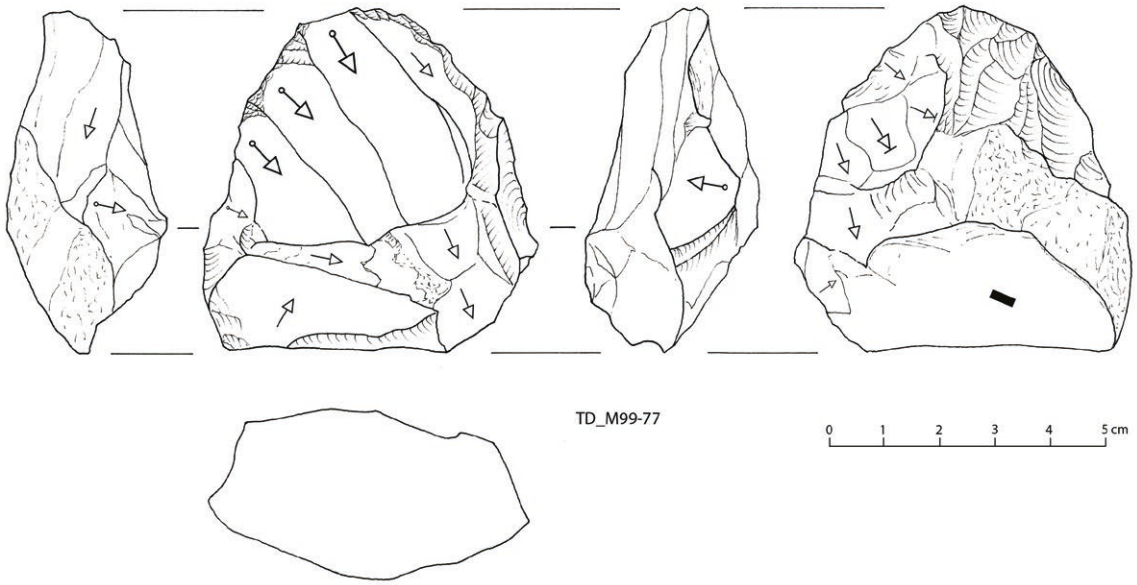

Fig. 13. Uni-directional blade core from the 2017 excavation.
Abb. 13. *Unidirektionaler Klingenkern, Grabung 2017.*

recovered (Fig. 17, M99-42, M101-25), notably three backed bladelets (Fig. 17, L99-74, L99-38) and one with an inversely retouched notch (Fig. 17, L99-94). A further three Dufour bladelets fragments were also found, one of which had only a single retouched side. A retouched notch on a bladelet was found. A final bladelet was a small "atypical" strangled blade fragment with light, invasive retouch (Fig. 17, M101-87).

The cortex percentage (Fig. 18) was recorded using the intervals 0, 1–10 %, 10–40 %, 40–60 %, 60–90 %, 90–99 % and 100 % for all pieces (for calculations the midpoint value of each interval was used i.e. 0.05 for 1–10 %, 0.25 for 10–40 %, etc.; flint density was set as 2.46 g/cm^3; Dibble et al. 2005). Formulas for the spherical nodule model were employed as it provides better results compared to cylindrical and tabular models (see discussion in Dibble et al. 2005 and Douglass et al. 2008). The cortex ratio of 0.53 suggests that the nodules were brought to the site after shaping, probably at the raw material source. This assumption is validated by the data presented that show the clear predominance of non-cortical pieces (Fig. 18). The presence of cores and core rejuvenation pieces indicates *in situ* exploitation. The scarcity of formal tools and the presence of a few burin spalls may indicate that the site was used as a workshop.

Discussion

Site formation processes

As no distinct archaeological levels could be identified, the homogeneous distribution of lithic material (Fig. 2) and scattered presence of rounded fluvial gravels may be explained by post-depositional reworking of the sediment. The homogeneity of the distribution agrees with the uniformity of geochemical parameters measured in the silty material. Due to reworking processes that included sediment mixing, the stratigraphic evidence is lost, along with geochemical signals.

However, the sedimentological proxies, together with the geochronological control reveal information about the post-depositional processes. The tri-modal grain size distribution (Fig. 4) represents the different phases of sedimentological site formation. The silt and the fine to medium sand modes are clear indicators for aeolian deposition of the material. Especially the sand mode is well-sorted which suggests windblown sand. The two shoulders within the silt mode do not necessarily reflect a sedimentological feature but could mirror the mineralogy and its effects on the diffraction behavior (Schulte et al. 2018). The coarse sand mode indicates syn- or post-sedimentary sheet wash accompanied by input of coarser particles and mixing of the material (e.g. Antoine et al. 2003). While the luminescence ages increase with depth and are in stratigraphic order, equivalent dose distributions scatter largely, which further points to a post-sedimentary disturbance, an overworking of the sediment, heterogeneous sediment composition or luminescence signal resetting. Simultaneously, the pOSL signals increase steadily with depth, but do not show any disturbances. However, varying signal intensities are easily obscured by the large amount of sample material that was used for pOSL. Finally, we suggest that the complex grain size distribution is likely caused by erosion and redeposition of the material by running water during the Holocene (as indicated by the OSL ages). The rather homogeneous distribution of lithic material contradicts a transport in a channel or creek, where the reworking would result in stratified artifacts. The

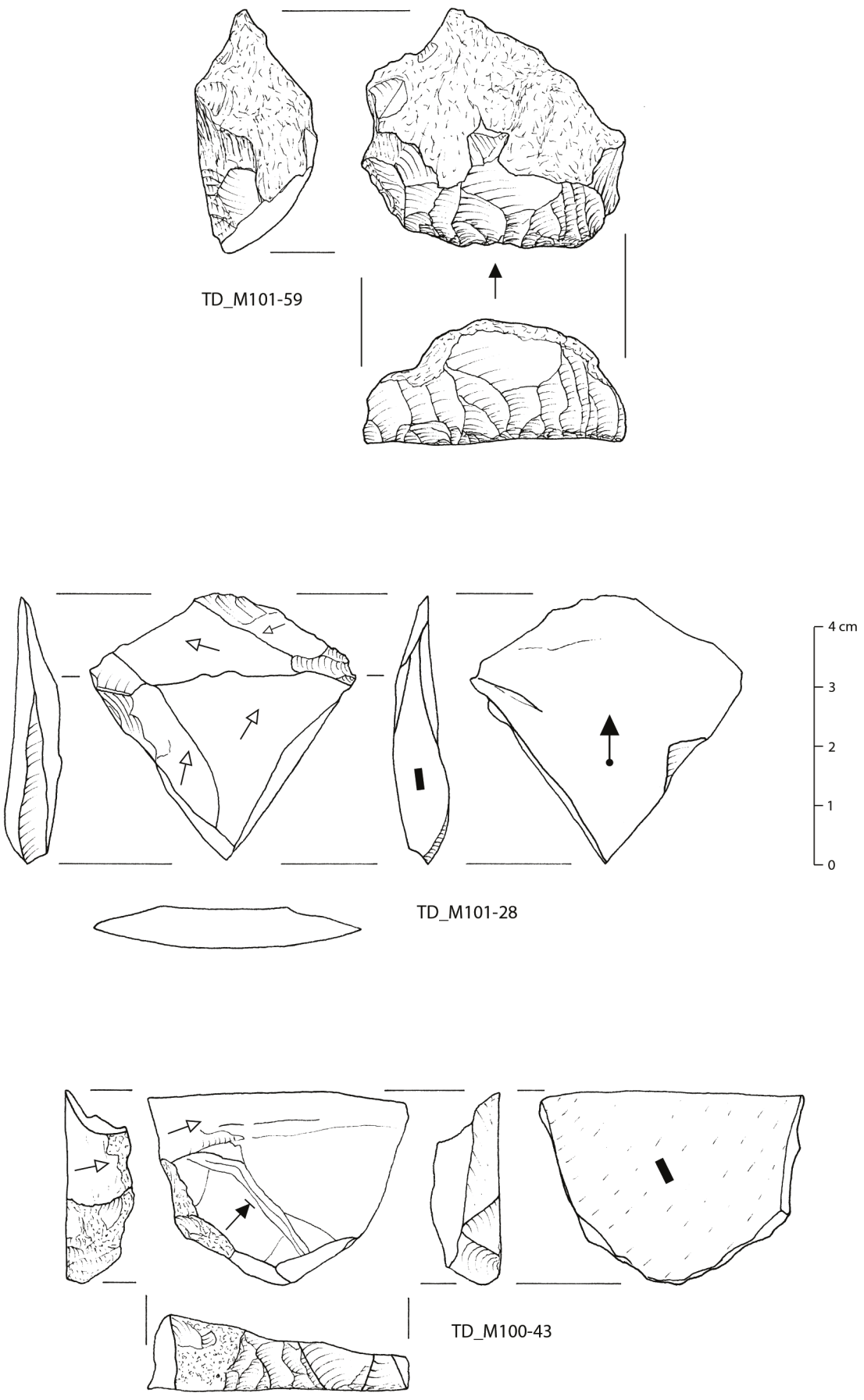

Fig. 14. Selection of tools from the 2017 excavation. M101-59: thick endscraper; M101-28: burin on break; M100-43: core tablet.
Abb. 14. *Werkzeuge der Grabung 2017 (Auswahl). M101-59: hoher Kratzer; M101-28: Stichel an Bruch; M100-43: Kernscheibe.*

Tool type	Subtype	N
Retouched blades/bladelets (12)	Dufour	3
	Backed	3
	Strangled	1
	Non-diagnostic	5
Endscrapers (10)	Simple	9
	With burin	1
Burins on break (2)		2
Retouched notch		1
Total		**25**

Fig. 15. Lithic tool types from the 2017 excavation.
Abb. 15. *Werkzeugtypen der Grabung 2017.*

consistent radiometric ages and, especially, the high-resolution pOSL-results indicate continuous, but small-scale relocation of the parent material by surface runoff. However, given the large amount of small knapping debitage and the relative fresh edges and aretes of the artifacts, it is likely that horizontal displacement on the scale of the terrace may be minimal.

Geochemical and sedimentological comparisons to other sites in the Bega Valley

Comparing Temereşti with the sites of Româneşti and Coşava (Kels et al. 2014), it is striking that Temereşti lacks a stratigraphic succession found at the other sites. The chemical composition of the Banat sites reveals a large overlap in many geochemical proxy ratios between the sites. Especially Temereşti and Coşava show similar patterns, particularly the ZrO_2/TiO_2, the Al_2O_3/K_2O and the Al_2O_3/TiO_2 ratios (Fig. 19). The data for Româneşti shows a significant overlap in those ratios, indicating a similar (or the same) source area of the parent material (Buggle et al. 2008; cf. Obreht et al. 2017). The MnO/Fe_2O_3 ratio is an indicator for redoximorphic features (Kels et al. 2014). It shows that the samples from Temereşti were not as strongly affected by these processes as the other two sites. Especially Româneşti shows a large scatter in both manganese and iron, indicating an influence by stagnant water, e.g. groundwater.

The outliers, which belong to Româneşti, can be explained with the differences in grain size between the two sites (Fig. 20). The site shows particularly high clay content. The sub-mode in the medium clay fraction indicates *in situ* formation of clay minerals and pedogenesis (Schulte & Lehmkuhl 2017). In Româneşti, the grain size distribution is much finer. The clay contents exceed 20 % and only one distinct mode in the coarse silt fraction is visible. Only a subordinate amount of medium sand is visible. Coşava shows a similar course within the grain size classes as Temereşti. Two modes are visible, one in the coarse silt and another, more pronounced one in the medium sand fraction. The mineralogical effects on the grain size correspond to those in Temereşti. The third mode seen, the coarse sand mode, is not visible in Coşava, since the samples from that site were sieved to just investigate the *in situ* material and avoid colluvial material in the coarse sand fraction.

The higher number of fine particles and distinct archaeological layers (Sitlivy et al. 2012; Kels et al. 2014), indicate higher landscape stability in Româneşti, compared to the sites of Coşava and Temereşti, which are more strongly influenced by reworking processes. The sand fraction in Româneşti is also poorly sorted, which also indicates reworking, but to a lesser extent than Coşava and Temereşti. These differences are *inter alia* due to the geomorphological position of the sites. Even though Temereşti and Româneşti are in comparable elevations, Coşava and Temereşti are more analogous regarding the terrace setting and the slope (Fig. 6). This indicates a more stable landscape in Româneşti during the Holocene. At Temereşti, the recent soil is also not preserved and probably eroded in large parts.

Archaeological comparisons with other open-air Upper Palaeolithic assemblages in the Bega Valley

At least two major technological groupings can be distinguished amongst the lithic inventories of Temereşti. For ease, they may be referred to as Aurignacian that is testified by the Dufour (subtype Dufour) bladelets and the "atypical" strangled blade and another (Epi-)Gravettian evidenced by the presence of typical backed bladelets. Such an interpretation would fit well within the typo-technological scheme of other local stratified archaeological assemblages at Româneşti and Coşava that preserve stratified Aurignacian and (Epi-)Gravettian assemblages in similar sediments. Given the morphology of the Dufour bladelets alone, such a scenario might echo the affinity to the Proto-Aurignacian character of Româneşti and the further afield Tincova for the earlier part (Teyssandier 2004; Sitlivy et al. 2012).

However, given the mechanical mixing of the site, it is clear that subsequent site formation processes created a palimpsest of artifacts and therefore isolating discrete assemblages that are manufactured on largely the same raw materials for comparisons remains difficult especially given the low number of formal tools and cores recovered. Still, some observations can be made with reference to the types of retouched tools found at the site. While tool forms and cores can be matched between Coşava and Româneşti, the relative proportions of these tools are notably different despite of mixing. While for instance, bladelet production predominates at Româneşti, there are few endscrapers. At Temereşti the inverse is true (Sitlivy et al. 2012). Such a difference may point to a different chronological/functional aspect of the site though given the absence of chronological markers for Temereşti, Tincova and Coşava and the lack of seasonal data (e.g. faunal remains), it is currently unreasonable to elaborate on any of these.

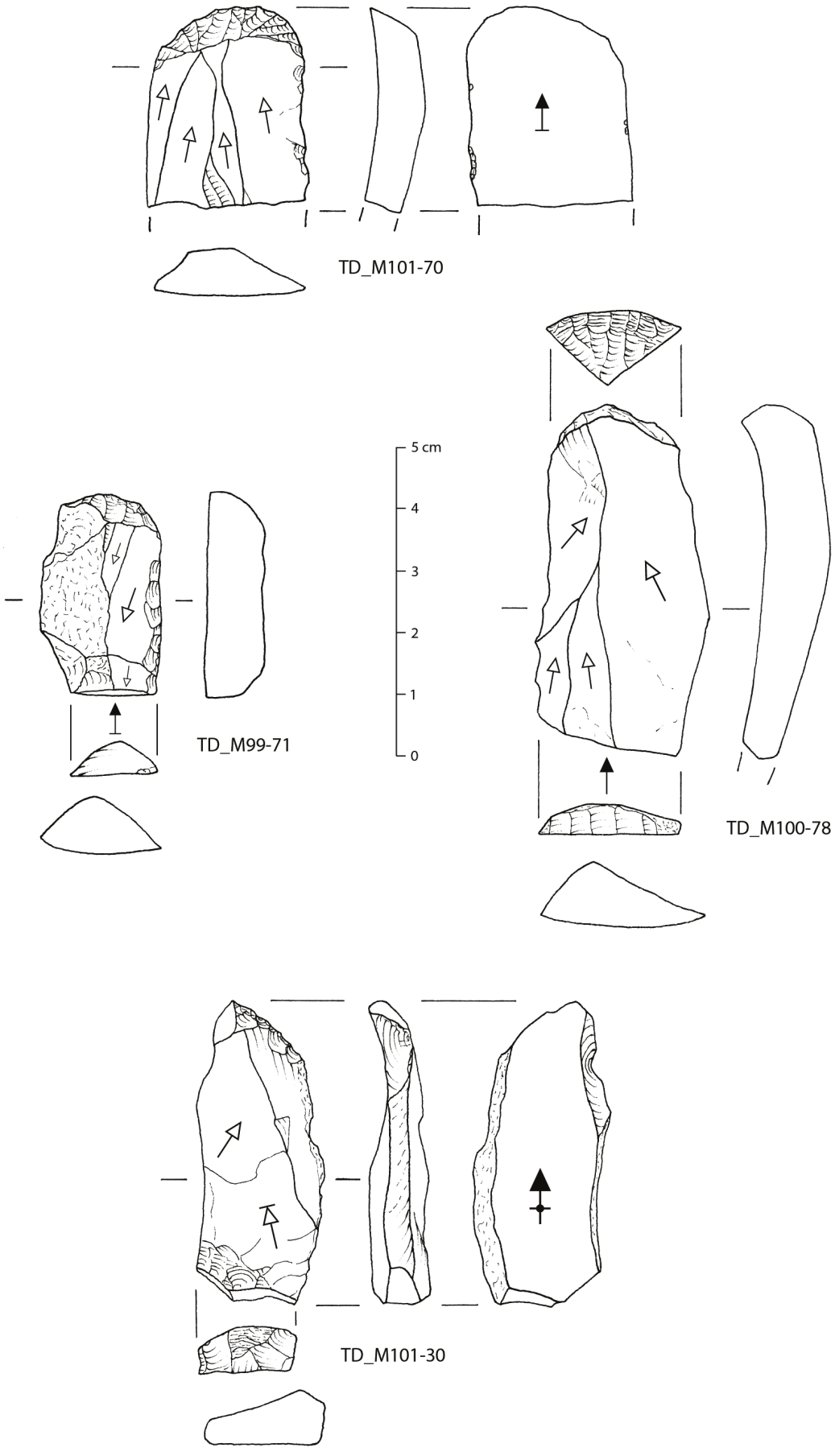

Fig. 16. Endscrapers from the 2017 excavation.
Abb. 16. *Klingenkratzer aus der Grabung 2017.*

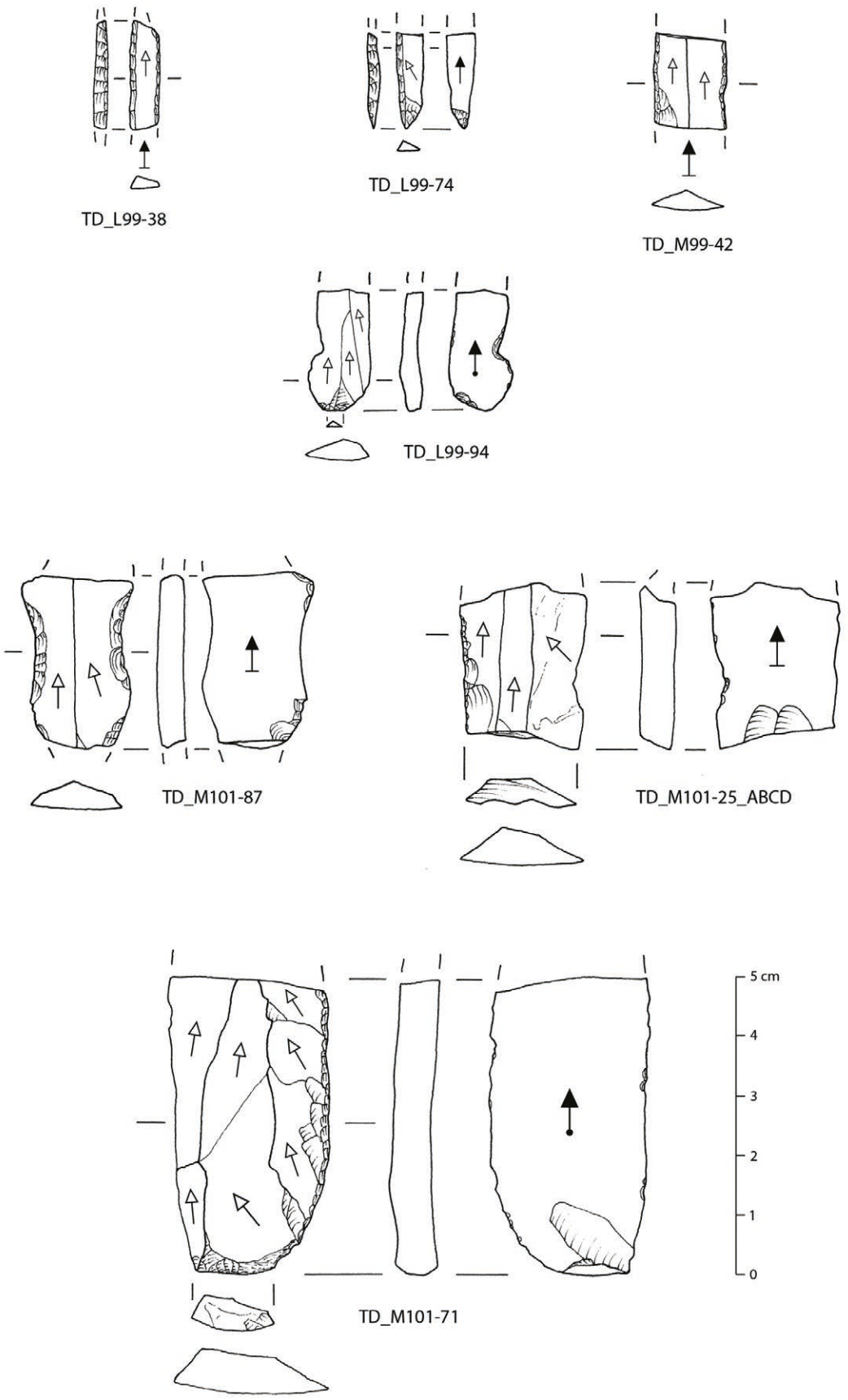

Fig. 17. Laterally retouched laminar blanks. L99-38 and L99-74: backed bladelets; M99-42: retouched bladelet; L99-94: bladelet with inversely retouched notch; M101-87: atypical strangled blade fragment; M101-25_ABCD and M101-71: retouched blades.

Abb. 17. *Lateralretuschierte Klingen und Lamellen. L99-38 und L99-74: Rückenmesser; M99-42: retuschierte Lamelle; L99-94: Lamelle mit Einkerbung (invers retuschiert); M101-87: untypische eingeschnürte Klinge (Medialfragment); M101-25_ABCD und M101-71: lateralretuschierte Klingen.*

Percentage of cortex	N
0	302
1-10 %	20
10-40 %	19
40-60 %	26
60-90 %	5
90-99 %	14
100 %	18
Indeterminate	12
Total	**416**

Fig. 18. Cortex percentages on lithic artifacts from single finds.
Abb. 18. *Kortexanteil an Silexartefakten aus Grabungskontext.*

Despite the palimpsest nature of the Temereşti assemblage, there are no indications of earlier typological assemblages such as the so-called Quartzite Mousterian (e.g. Pop 2013: 27–28) found at Românești that is also notably absent at Coşava and Tincova. While it is possible that the limited extent of our excavations and the relative thinness of the layer at Românești cannot preclude simply having "missed" these artifacts, it may also be in line with the notion that earlier human populations (presumably Neandertals) in Southeastern Europe may not have been in direct ecological competition with the makers of the early Upper Palaeolithic (Alex et al. 2019; Mihailović 2020). Another alternative model is that

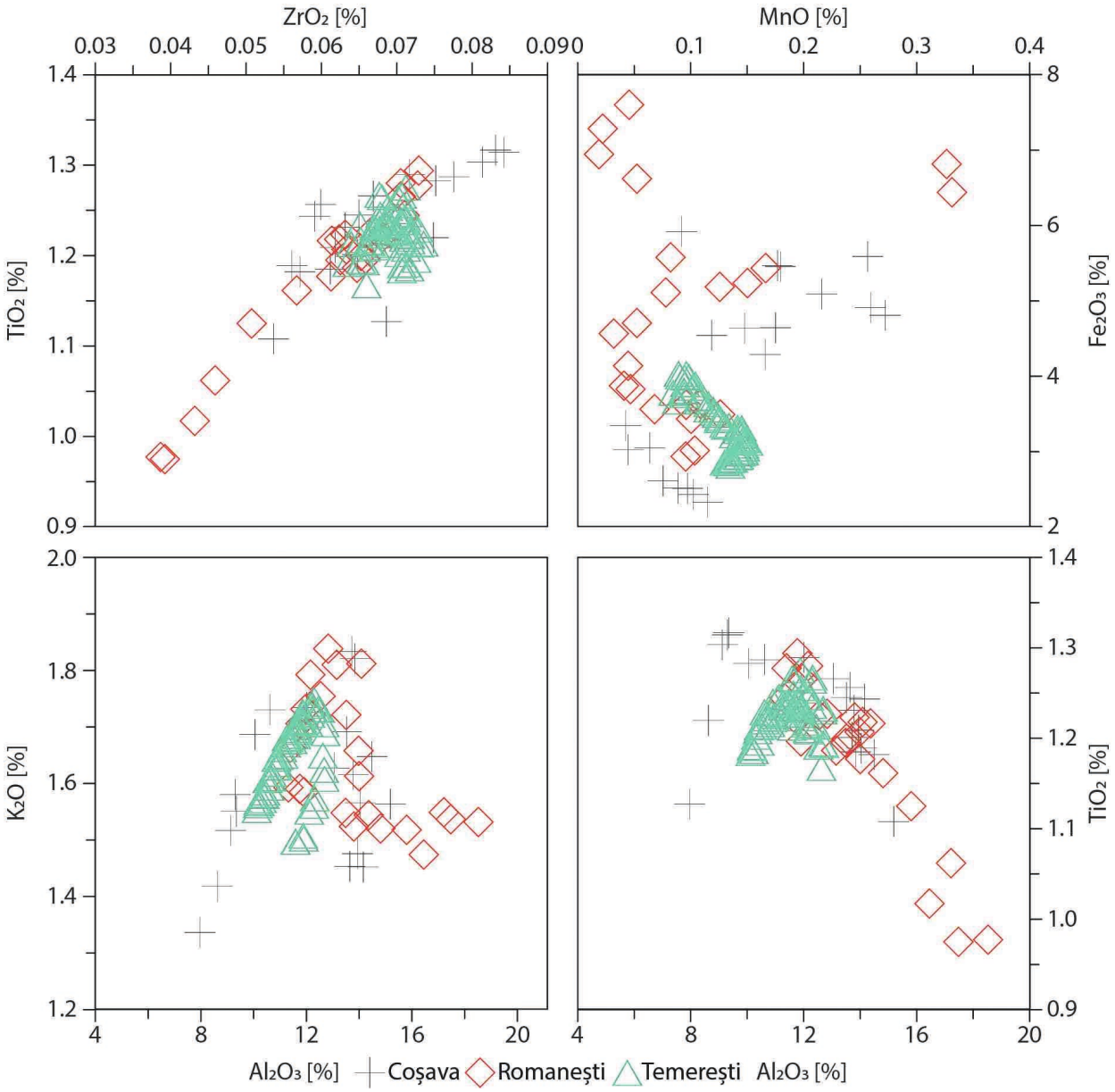

Fig. 19. Bi-plots of different oxides for Românești, Coşava and Temereşti.
Abb. 19. *Streudiagramme verschiedener Oxide für Românești, Coşava und Temereşti.*

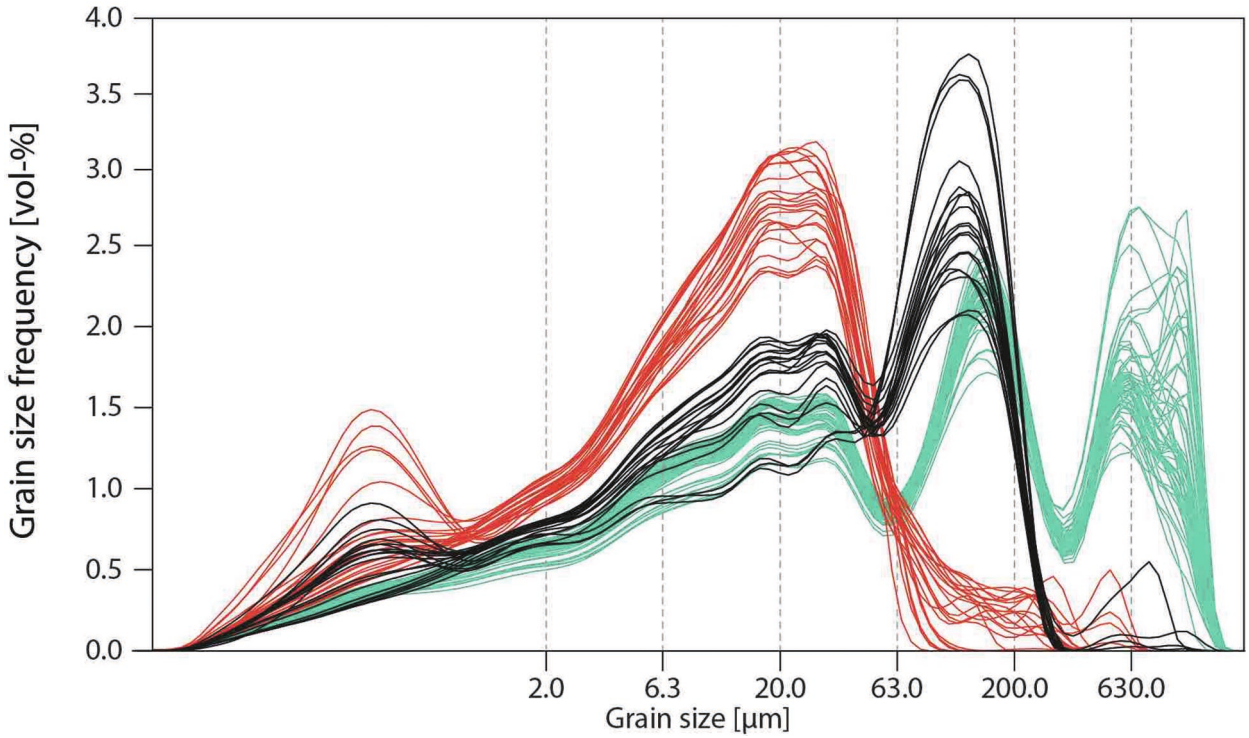

Fig. 20. Grain size distributions of Românești (red), Coșava (black) and Temereşti (green). Note that for Coșava the coarse sand fraction was separated before grain size analysis.

Abb. 20. *Korngrößenverteilungen für Românești (rot), Coșava (schwarz) und Temereşti (grün). Die Grobsandfraktion für Coșava wurde vor der Korngrößenanalyse abgesiebt.*

the regional changes from the Middle to Upper Palaeolithic transition is less bioculturally driven and more the result of increasing logistic mobility (Riel-Salvatore et al. 2008) triggered by increasingly challenging climatic conditions (Staubwasser et al. 2018). Given roughly contemporaneous hybridization of the Peştera cu Oase fossils however, a likelier scenario may suggest that neither of these two models are mutually exclusive (Fu et al. 2015).

Whatever the outcome of these models, our results suggest that along the Bega and in the wider Banat region, terrace localities were persistence places throughout the early Upper Palaeolithic frequently reoccupied for a variety of purposes. This is in contrast to other localities such as in caves that appear to have been less intensively occupied for a more limited range of activities as evidenced by the near absence of Upper Palaeolithic artifacts at the nearby hominin bearing sites of Peştera cu Oase, Peştera Muierii, Peştera Cioclovina and Bordul Mare (Fig. 1; Nicolăescu-Plopşor et al. 1957; Trinkaus et al. 2003b; Harvati et al. 2007; Doboş et al. 2010). This implicates an increased importance of riparian landscapes during the Late Pleistocene not only as a source of water and raw materials, but as a potential supply for a broader dietary range that may have included freshwater resources (Richards & Trinkaus 2009; Trinkaus et al. 2009).

Conclusion

Small-scale excavations at the site of Temereşti have revealed a well defined though typologically heterogeneous artifact cluster in a region increasingly known for its rich Late Pleistocene/early Upper Palaeolithic archaeological and palaeontological record. In spite of a large density of archaeological finds, the site experienced sediment reworking at the latest during the Holocene as shown by granulometry, geochemistry and radiometric dating as well as the lack of any clear archaeological stratigraphy. The reworking points to persistent landscape instability during the Holocene, since the proxy data indicates (sub-)continuous mixing of the sediment. Still, the geographic position, embedding sediments and lithic artifact forms correspond to stratified and radiometrically dated Aurignacian/(Epi-)Gravettian sites in the Bega River system and are most parsimoniously contemporaneous.

The use of local raw materials, high amount of debitage and low formal tool count points to a larger regional occupation during the early Upper Palaeolithic on terrace localities that were frequently re-occupied, probably primarily for artifact retooling, possibly as a result of increased climatically-driven logistic mobility strategies. Connecting this region to other better known regions remains a main goal for future work and larger studies may help integrate the better known contemporary early Upper Palaeolithic records to the east and west.

Acknowledgements: This research was funded by the Deutsche Forschungsgemeinschaft (DFG, German Research Foundation) - Project Number 57444011 - SFB 806. The authors would like to thank Anja Rüschmann for providing artifact illustrations, Marianne Dohms for processing sediment samples, Anja Zander for the dosimetry measurements and Elena-Cristina Nițu for her advice about the site. *Mulțumesc* to Andrei Balarie, Cristine Harnischferger and the staff of the Banat Museum for their logistical support. We are indebted to Florin Frunzea and Sergiu Munteanu for assistance. *In memory of Alexandru Szentmiklosi.*

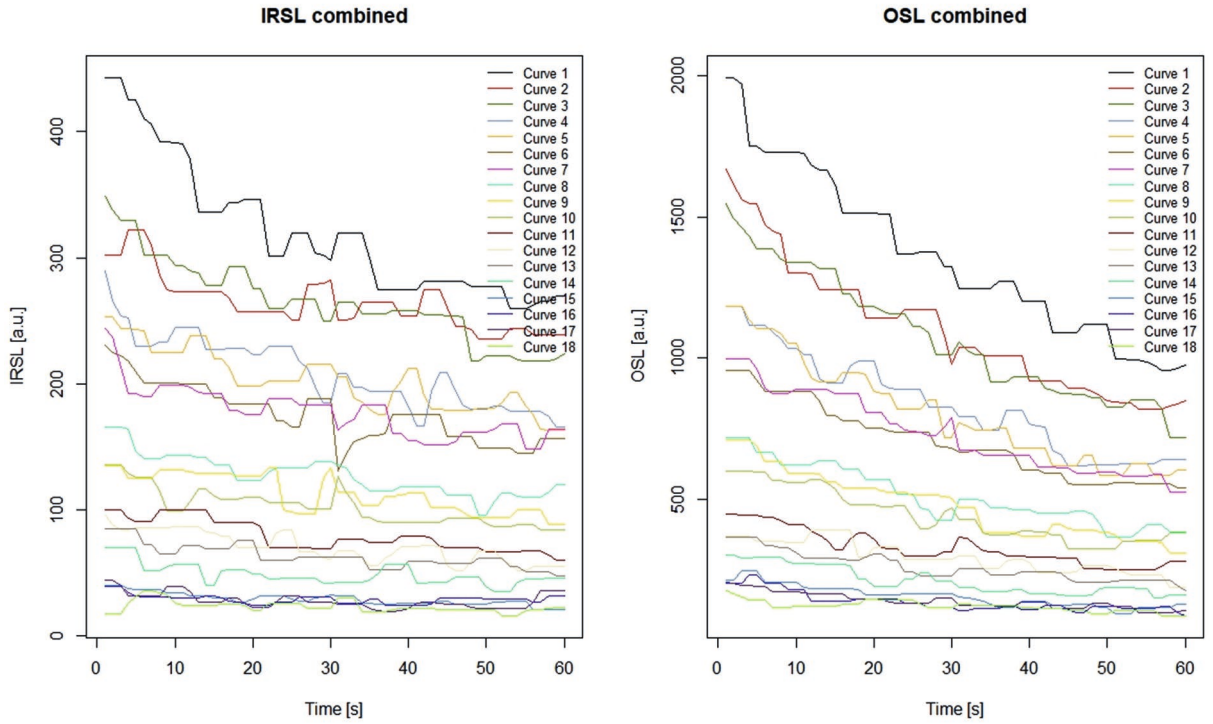

Appendix, Plate 1. Signals of pOSL measurements on unprepared samples showing all samples from curve 1 (lowermost sample pOSL18) to curve 18 (uppermost sample pOSL1). Plot generated using the analyse_portableOSL function in the R "luminescence" package (Burow et al. 2018).

Appendix, Tafel 1. *Signale der pOSL-Messungen an unaufbereiteten Proben. Dargestellt sind alle Proben von Kurve 1 (unterste Probe pOSL 18) bis Kurve 18 (oberste Probe pOSL 1). Die Abb. wurde mit der Funktion analyse_portableOSL des R-Pakets „luminescence" (Burow et al. 2018) erstellt.*

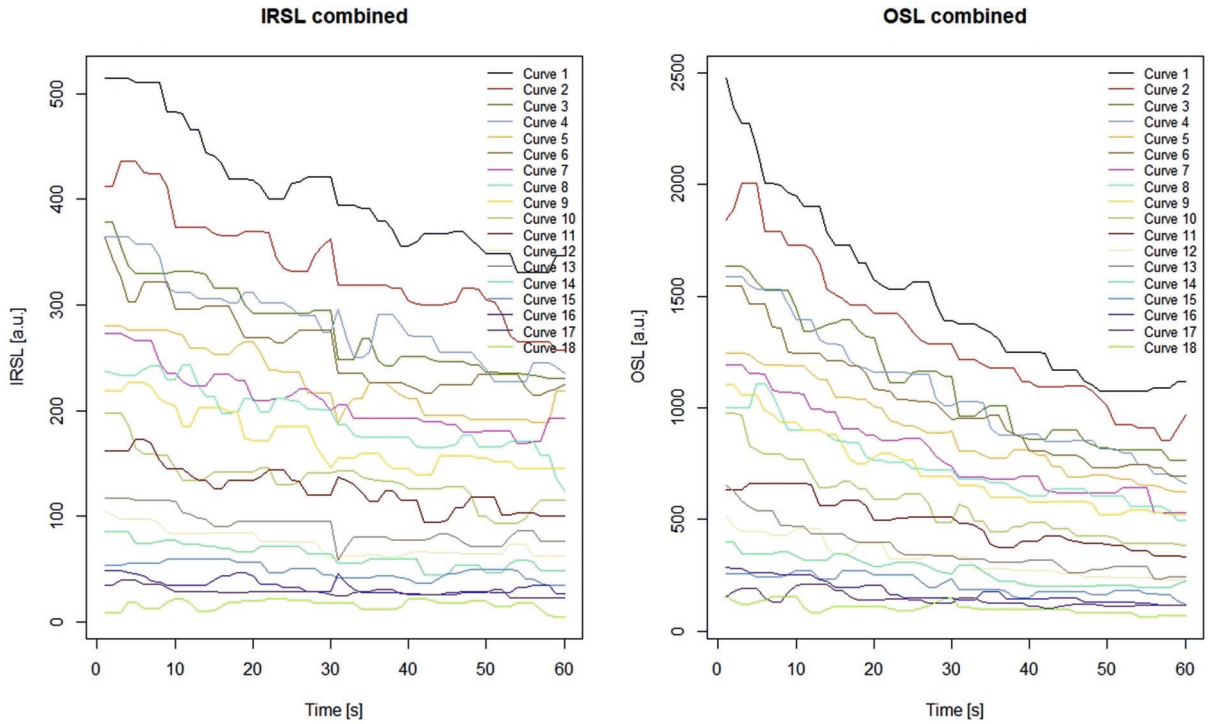

Appendix, Plate 2. Signals of pOSL measurements on crushed samples showing all samples from curve 1 (lowermost sample pOSL18) to curve 18 (uppermost sample pOSL1). Plot generated using the analyse_portableOSL function in the R "luminescence" package (Burow et al. 2018).

Appendix, Tafel 2. *Signale der pOSL-Messungen an gemörserten Proben. Dargestellt sind alle Proben von Kurve 1 (unterste Probe pOSL 18) bis Kurve 18 (oberste Probe pOSL 1). Die Abbildung wurde mit der Funktion analyse_portableOSL des R-Pakets „luminescence" (Burow et al. 2018) erstellt.*

		Unprepared samples		Crushed samples		Unprepared samples		Crushed samples	
Sample	Depth (cm)	BSL (counts)	BSL st.dev.	BSL (counts)	BSL st.dev.	IRSL (counts)	IRSL st.dev.	IRSL (counts)	IRSL st.dev.
pOSL1	10	715.5	67.5	735.5	73.5	99	12	75.5	73.5
pOSL2	12.75	873	113	1 114.5	211.5	151.5	40.5	211	211.5
pOSL3	15.75	1 065.5	0.5	1 364.5	4.5	173.5	9.5	244	4.5
pOSL4	18.5	1 082.5	79.5	1 423.5	145.5	206	11	277.5	145.5
pOSL5	20.75	1 342	139	1 774	68	310	40	348	68
pOSL6	22.5	1 749	86	2 540	420	391	34	492	420
pOSL7	25	1 823	4	2 404.5	93.5	414.5	23.5	498.5	93.5
pOSL8	27.25	2 221.5	1.5	3 284.5	59.5	459.5	24.5	769.5	59.5
pOSL9	29	2 832	169	4 032.5	527.5	611	52	880	527.5
pOSL10	31.25	3 526	6	4 448.5	926.5	696.5	41.5	918.5	926.5
pOSL11	33.75	3 649	105	5 324	219	753	56	1 122.5	219
pOSL12	36	4 618.5	332.5	6 112.5	231.5	991.5	86.5	1 348	231.5
pOSL13	38	4 926	180	7 324.5	246.5	1 094	12	1 522.5	246.5
pOSL14	40.5	5 392.5	403.5	6 789	604	1 146	91	1 423.5	604
pOSL15	44	5 547.5	240.5	7 889.5	44.5	1 279	13	1 715	44.5
pOSL16	48	6 867	458	7 846.5	227.5	1 556	121	1 684.5	227.5
pOSL17	51.5	6 945.5	997.5	8 703	1 046	1 325	225	1 904.5	1 046
pOSL18	54	8 975	483	11 733.5	192.5	1 894	285	2 552	192.5

Appendix, Tab 3. Data from portable OSL reader measurements showing the depths of each sample, the counts and standard deviation (n = 2) of the unprepared and crushed samples for blue stimulated luminescence and infrared stimulated luminescence.

Appendix, Tab 3. *Daten der portablen OSL-Messungen für blau- und infrarot-stimulierte Lumineszenz mit Tiefenangaben zu jeder Probe, den Zählungen sowie der Standardabweichung (n = 2) für die nicht aufbereiteten und die gemörserten Proben.*

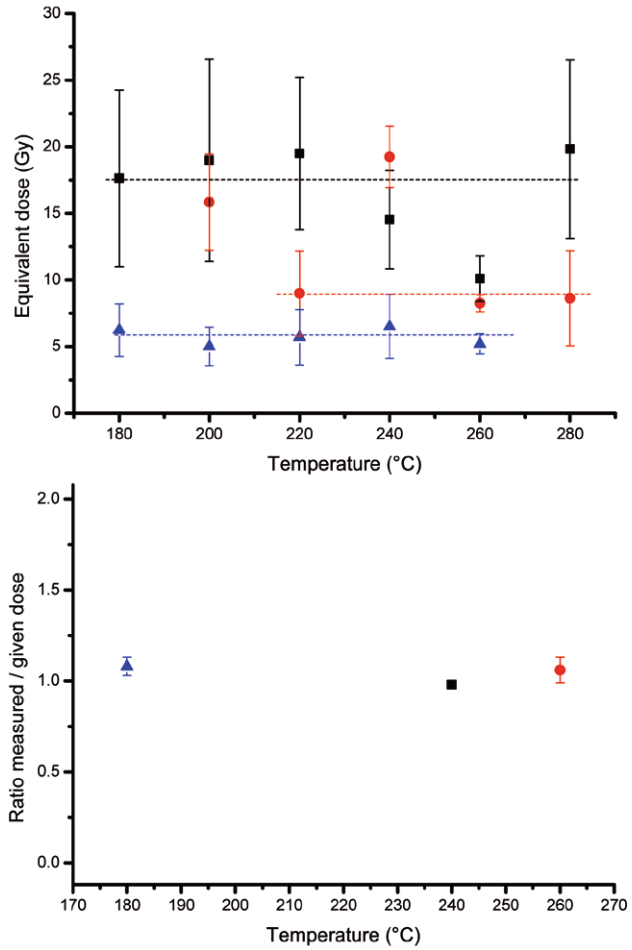

Appendix, Plate 4. Preheat plateau (top) and dose recovery test (bottom) of quartz OSL samples C-L4769 (black), C-L4770 (red), C-L4771 (blue).

Appendix, Tafel 4. *Vorwärm-Plateau- (oben) und Dose Recovery Tests (unten) der Quarzproben C-L4769 (schwarz), C-L4770 (rot) und C-L4771 (blau).*

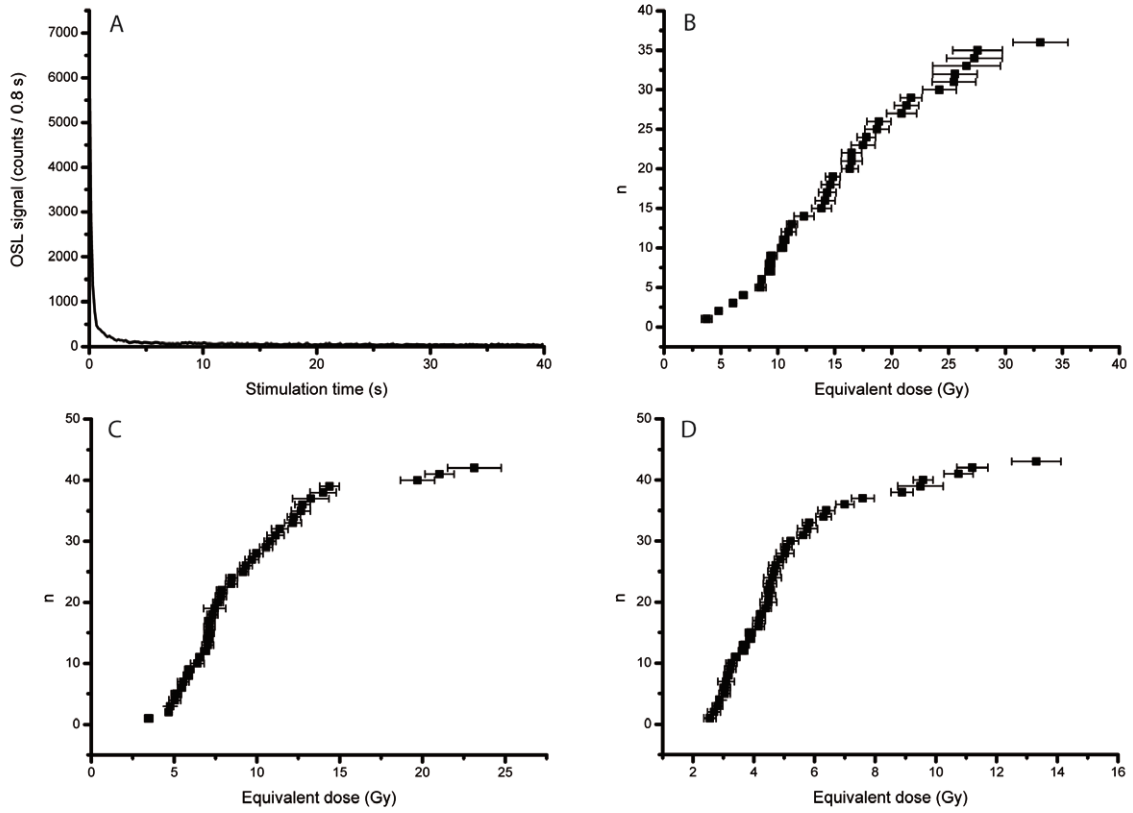

Appendix, Plate 5. A. Representative decay curve of luminescence sample C-L4769 measured on a 1 mm aliquots of 100–150 µm quartz. B–D. Equivalent dose distributions of C-L4769 (B), C-L4770 (C), and C-L4771 (D), measured on 1 mm aliquots.

Appendix, Tafel 5. *A Repräsentative Zerfallskurven für die Lumineszenzprobe C-L4769, gemessen an einem 1 mm Quarzaliquot mit einer Korngröße von 100–150 µm. B-D: Equivalenzdosenverteilungen für C-L4769 (B), C-L4770 (C) und C-L4771, gemessen an einem 1 mm Aliquot.*

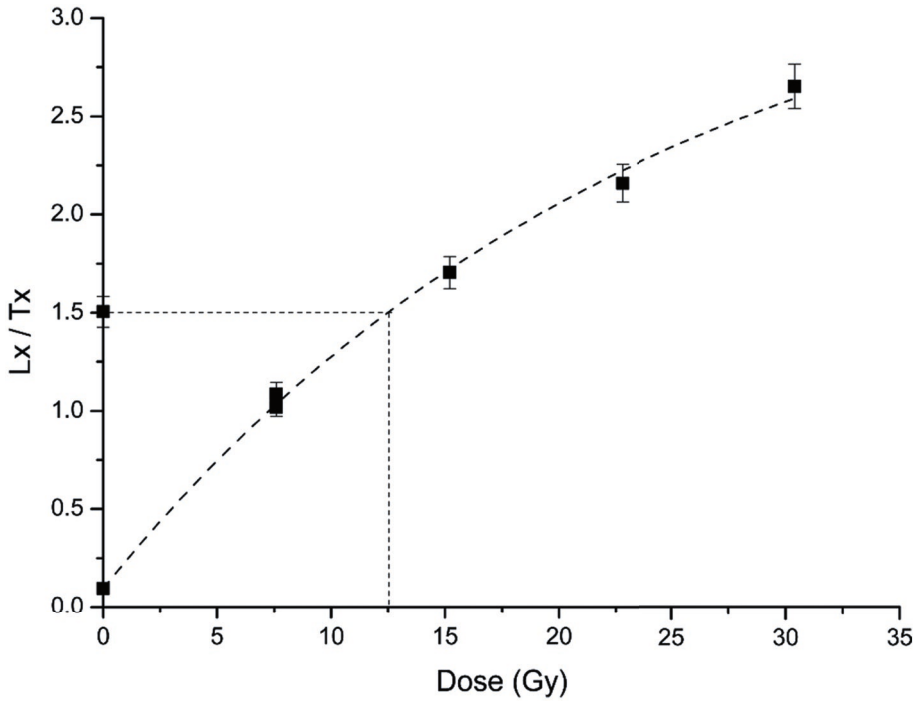

Appendix, Plate 6. Representative dose response curve of sample C-L4769.

Appendix, Tafel 6. *Repräsentative Aufbaukurve für die Probe C-L4769.*

Literature cited

Alex, B., Mihailović, D., Milošević, S. & Boaretto, E. (2019). Radiocarbon chronology of Middle and Upper Paleolithic sites in Serbia, Central Balkans. *Journal of Archaeological Science: Reports* 25: 266–279.

Allen, J. R. L. & Thornley, D. M. (2004). Laser granulometry of Holocene estuarine silts: Effects of hydrogen peroxide treatment. *The Holocene* 14 (2): 290–295.

Anghelinu, M. & Niţă, L. (2014). What's in a name: The Aurignacian in Romania. *Quaternary International* 351: 172–192.

Anghelinu, M., Niţă, L., Sitlivy, V., Uthmeier, T. & Băltean, I. (2012). Looking around Peştera Cu Oase: The beginnings of Upper Paleolithic in Romania. *Quaternary International* 274: 136–157.

Antoine, P., Catt, J., Lautridou, J.-P. & Sommé, J. (2003). The loess and coversands of northern France and southern England. *Journal of Quaternary Science* 18 (3–4): 309–318.

Bronk Ramsey, C., Higham, T. F. G., Brock, F., Baker, D. & Ditchfield, P. (2009). Radiocarbon dates from the Oxford AMS system: Archaeometry datelist 33. *Archaeometry* 51 (2): 323–349.

Buggle, B., Glaser, B., Zöller, L., Hambach, U., Marković, S., Glaser, I. & Gerasimenko, N. (2008). Geochemical characterization and origin of Southeastern and Eastern European loesses (Serbia, Romania, Ukraine). *Quaternary Science Reviews* 27 (9–10): 1058–1075.

Burow, C. (2018). Analyse_portableOSL(): Analyse portable CW-OSL measurements. Function version 0.0.3. *In*: S. Kreutzer, C. Burow, M. Dietze, M.C. Fuchs, C. Schmidt, M. Fischer & J. Friedrich (2018). *Luminescence: Comprehensive Luminescence Dating Data Analysis. R package version 0.9.0*. https://CRAN.R-project.org/package=Luminescence.

Chu, W. (2018). The Danube Corridor Hypothesis and the Carpathian Basin: Geological, environmental and archaeological approaches to characterizing Aurignacian dynamics. *Journal of World Prehistory* 31 (2): 117–178.

Chu, W., Hauck, T. & Mihailović, D. (2014). Crvenka-At–preliminary results from a lowland Aurignacian site in the middle Danube catchment. *In*: D. Mihailović (Ed.). *Palaeolithic and Mesolithic Research in the Central Balkans*. Serbian Archaeological Society, Belgrade, 69–75.

Comşa, E. (1971). Silexul de tip "Bănăţean". *Apulum* 9: 15–19.

Debénath, A. & Dibble, H. L. (1994). *Handbook of Paleolithic typology*. University Museum Press, Philadelphia.

Demars, P.-Y. (1992). L'Aurignacien ancien en Périgord. Le problème du Protoaurignacien. *Paléo* 4 (1): 101–122.

Dibble, H. L., Schurmans, U. A., Iovita, R. P. & McLaughlin, M. V. (2005). The measurement and interpretation of cortex in lithic assemblages. *American Antiquity* 70 (3): 545–560.

Doboş, A., Soficaru, A., Popescu, A. & Trinkaus, E. (2009). Radiocarbon dating and faunal stable isotopes for the Galeria Principala, Peştera Muierii, Baia de Fier, Gorj County, Romania. *Materiale şi Cercetari Arheologice* 5: 15–20.

Doboş, A., Soficaru, A. & Trinkaus, E. (2010). *The prehistory and paleontology of the Pestera Muierii (Romania)*. Université de Liège, Liège.

Douglass, M. J., Holdaway, S. J., Fanning, P. C. & Shiner, J. I. (2008). An assessment and archaeological application of cortex measurement in lithic assemblages. *American Antiquity* 73 (3): 513–526.

Duller, G. A. T. (2003). Distinguishing quartz and feldspar in single grain luminescence measurements. *Radiation Measurements* 37: 161–165.

Durcan, J. A., King, G. E. & Duller, G. A. T. (2015). DRAC: Dose rate and age calculator for trapped charge dating. *Quaternary Geochronology* 28: 54–61.

Fu, Q., Hajdinjak, M., Moldovan, O. T., Constantin, S., Mallick, S., Skoglund, P., Patterson, N., Rohland, N., Lazaridis, I., Nickel, B., Viola, B., Prüfer, K., Meyer, M., Kelso, J., Reich, D. & Pääbo, S. (2015). An early modern human from Romania with a recent Neanderthal ancestor. *Nature* 524 (7564): 216–219.

Guérin, G., Mercier, N. & Adamiec, G. (2011). Dose-rate conversion factors: Update. *Ancient TL* 29 (1): 5–8.

Harvati, K., Gunz, P. & Grigorescu, D. (2007). Cioclovina (Romania): Affinities of an early modern European. *Journal of Human Evolution* 53 (6): 732–746.

Hiscock, P. (2002). Quantifying the size of artefact assemblages. *Journal of Archaeological Science* 29 (3): 251–258.

Inizan, M.-L., Reduron-Ballinger, M., Roche, H. & Tixier, J. (1999). *Technology and terminology of knapped stone*. Préhistoire de la Pierre Taillée 5, CREP, Nanterre.

JAXA EORC. (2016). ALOS Global Digital Surface Model "ALOS World 3D - 30m" (AW3D30).

Kels, H., Protze, J., Sitlivy, V., Hilgers, A., Zander, A., Anghelinu, M., Bertrams, M. & Lehmkuhl, F. (2014). Genesis of loess-like sediments and soils at the foothills of the Banat Mountains, Romania – Examples from the Paleolithic sites Românești and Coşava. *Quaternary International* 351: 213–230.

Micle, D., Cârciumaru, M., Niţu, E.-C., Stavilă, A. & Dinca, R. (2015). 110. Temereşti, oraşul Făget, Jud. Timiş Punct: Dealu Vinii. *Cronica Cercetărilor Arheologice Din România - Campania* 2015: 205–207.

Mihailović, D. (2020). Push-and-pull factors of the Middle to Upper Paleolithic transition in the Balkans. *Quaternary International* 551: 47-62.

Mogoşanu, F. (1978). *Paleoliticul din Banat* (Vol. 32). Bucharest: Editura Academiei Republicii Socialiste România.

Murray, A. S. & Wintle, A. G. (2000). Luminescence dating of quartz using an improved single-aliquot regenerative-dose protocol. *Radiation Measurements* 32: 57–73.

Murray, A. S. & Wintle, A. G. (2003). The single aliquot regenerative dose protocol: Potential for improvements in reliability. *Radiation Measurements* 37 (4): 377–381.

Nicolăescu-Plopşor, C. S., Haas, N., Paunescu, A. & Bolomey, A. (1957). Santierul arheologic Ohaba Ponor. *Materiale şi Cercetari Arheologice* 3: 41–49.

Nottebaum, V., Stauch, G., Hartmann, K., Zhang, J. & Lehmkuhl, F. (2015). Unmixed loess grain size populations along the northern Qilian Shan (China): Relationships between geomorphologic, sedimentologic and climatic controls. *Quaternary International* 372: 151–166.

Obreht, I., Hambach, U., Veres, D., Zeeden, C., Bösken, J., Stevens, T., Marković, S. B., Klasen, N., Brill, D., Burow, C. & Lehmkuhl, F. (2017). Shift of large-scale atmospheric systems over Europe during late MIS 3 and implications for Modern Human dispersal. *Scientific Reports* 7 (1): 5848.

Özer, M., Orhan, M. & Işik, N. S. (2010). Effect of particle optical properties on size distribution of soils obtained by laser diffraction. *Environmental & Engineering Geoscience* 16 (2): 163–173. Pop, C. (2013). *The Middle Palaeolithic of present day Romania: A critical review.* M.A., thesis, University of British Columbia, Vancouver.

Prescott, J. R. & Hutton, J. T. (1994). Cosmic ray contributions to dose rates for luminescence and ESR dating: Large depths and long-term time variations. *Radiation Measurements* 23 (2–3): 497–500.

Reimer, P. J., Bard, E., Bayliss, A., Beck, J. W., Blackwell, P. G., Bronk Ramsey, C., Buck, C. E., Cheng, H., Edwards, R. L., Friedrich, M., Grootes, P. M., Guilderson, T. P., Haflidason, H., Hajdas, I., Hatté, C., Heaton, T. J., Hoffmann, D. L., Hogg, A. G., Hughen, K. A., Kaiser, K. F., Kromer, B., Manning, S. W., Niu, M., Reimer, R. W., Richards, D. A., Scott, E. M., Southon, J. R., Staff, R. A., Turney, C. S. M. & van der Plicht, J. (2013). IntCal13 and Marine13 radiocarbon age calibration curves 0–50,000 years cal BP. *Radiocarbon* 55 (4): 1869–1887.

Richards, M. P. & Trinkaus, E. (2009). Isotopic evidence for the diets of European Neanderthals and early modern humans. *Proceedings of the National Academy of Sciences* 106: 16034–16039.

Riel-Salvatore, J., Popescu, G. & Barton, C. M. (2008). Standing at the gates of Europe: Human behavior and biogeography in the Southern Carpathians during the Late Pleistocene. *Journal of Anthropological Archaeology* 27 (4): 399–417.

Sanderson, D. C. W. & Murphy, S. (2010). Using simple portable OSL measurements and laboratory characterisation to help understand complex and heterogeneous sediment sequences for luminescence dating. *Quaternary Geochronology* 5 (2–3): 299–305.

Schulte, P. & Lehmkuhl, F. (2017). The difference of two laser diffraction patterns as an indicator for post-depositional grain size reduction in loess-paleosol sequences. *Palaeogeography, Palaeoclimatology, Palaeoecology* 509: 126–136.

Schulte, P., Lehmkuhl, F., Steininger, F., Loibl, D., Lockot, G., Protze, J., Fischer, P. & Stauch, G. (2016). Influence of HCl pretreatment and organo-mineral complexes on laser diffraction measurement of loess–paleosol-sequences. *CATENA* 137: 392–405.

Schulte, P., Sprafke, T., Rodrigues, L. & Fitzsimmons, K. E. (2018). Are fixed grain size ratios useful proxies for loess sedimentation dynamics? Experiences from Remizovka, Kazakhstan. *Aeolian Research* 31: 131–140.

Sitlivy, V., Chabai, V., Anghelinu, M., Uthmeier, T., Kels, H., Hilgers, A., Schmidt, C., Niţă, L., Băltean, I., Veselsky, A. & Hauck, T. (2012). The earliest Aurignacian in Romania: New investigations at the open air site of Românești-Dumbrăviţa I (Banat). *Quartär* 59: 85–130.

Sitlivy, V., Chabai, V., Anghelinu, M., Uthmeier, T., Kels, H., Niţă, L., Băltean, I., Veselsky, A. & Ţuţu, C. (2014). Preliminary reassessment of the Aurignacian in Banat (south-western Romania). *Quaternary International* 351: 193–212.

Staubwasser, M., Drăguşin, V., Onac, B. P., Assonov, S., Ersek, V., Hoffmann, D. L. & Veres, D. (2018). Impact of climate change on the transition of Neanderthals to modern humans in Europe. *Proceedings of the National Academy of Sciences* 115 (37): 9116.

Tasić, N. & Draşovean, F. (Eds.) (2011). *The Prehistory of Banat: The Palaeolithic and Mesolithic*. Publishing House of the Romanian Academy, Bucharest.

Teyssandier, N. (2004). *Les débuts de l'Aurignacien en Europe: Discussion à partir des sites de Geissenklösterle, Willendorf II, Krems-Hundssteig et Bacho Kiro*. Ph.D. thesis, Université Paris X-Nanterre, Paris.

Trinkaus, E., Constantin, S. & Zilhão, J. (2012). *Life and death at the Peştera cu Oase: A setting for modern human emergence in Europe.* Oxford University Press, New York.

Trinkaus, E., Milota, Ş., Rodrigo, R., Mircea, G. & Moldovan, O. (2003a). Early modern human cranial remains from the Peştera cu Oase, Romania. *Journal of Human Evolution* 45 (3): 245–253.

Trinkaus, E., Moldovan, O., Milota, Ş., Bîlgăr, A., Sarcina, L., Athreya, S., Bailey, S. E., Rodrigo, R., Mircea, G., Higham, T., Bronk Ramsey, C. & van der Plicht, J. (2003b). An early modern human from the Peştera cu Oase, Romania. *Proceedings of the National Academy of Sciences* 100 (20): 11231–11236.

Trinkaus, E., Soficaru, A., Doboş, A., Constantin, S., Zilhão, J. & Richards, M. (2009). Stable isotope evidence for early modern human diet in Southeastern Europe: Peştera cu Oase, Peştera Muierii and Peştera Cioclovina Uscată. *Materiale şi Cercetări Arheologice* 5: 4–14.